Thermodynamic analysis and material design to enhance chemo-mechanical coupling in hydrogels for energy harvesting from salinity gradients

Thermodynamic Analysis and Material Design to Enhance Chemo-Mechanical Coupling in Hydrogels for Energy Harvesting from Salinity Gradients

Sui Zhang[1,2,*], Shaoting Lin[1], Xuanhe Zhao[1], Rohit Karnik[1,*]

[1]Department of Mechanical Engineering, Massachusetts Institute of Technology, 77 Massachusetts Ave, Cambridge, MA 02139, USA.

[2]Department of Chemical and Biomolecular Engineering, National University of Singapore, 4 Engineering Drive 4, Singapore 117585, Singapore.

[*]Corresponding authors:
Dr. Sui Zhang, Email: chezhangsui@nus.edu.sg, Phone: 65-65163781;
Prof. Rohit Karnik, Email: karnik@mit.edu, Phone: 1- 617-324-1155.

Abstract

The coupling between solution salinity and the mechanics of charged hydrogels presents an opportunity to harvest osmotic energy in a clean and sustainable way. By applying mechanical pressure to retard the swelling or deswelling of hydrogels in saline solutions, the free energy of mixing is converted to mechanical work. This study developed a theoretical framework and experimentally investigated the potential of hydrogels for energy production from salinity gradients. Mathematical modeling revealed the effect of parameters including the charge and elastic modulus of hydrogels, applied pressure, and the solution salinity on energy conversion using different thermodynamic cycles. With proper material design and process control, the thermodynamic efficiency of an ideal process was predicted to exceed 5% with 10 mM and 600 mM NaCl solutions. Experiments with poly (styrene sulphonate) (PSS) hydrogels verified the theoretically predicted trends and demonstrated more than 10% thermodynamic efficiency for moderate-salinity sources, due to the unique swelling-strengthened mechanical properties of the gels. The study suggests the potential of polyelectrolyte hydrogels for extraction of energy from low- to moderate-salinity sources and provides a framework for their design.

Nomenclature

μ	Chemical potential	R	Universal gas constant
A	Quasilattice parameter	r	Nearest neighbor distance
b	Bond length of ideal polymer chain	T	Temperature
B_1	Numerical factor for swelling kinetics	V	Volume
C	Concentration	v	Molar volume
C_{ratio}	Concentration of salt penetrating into the gel relative to that in bath	W	Work
D	Gel bead diameter	W_{max}	Maximum work in zero-friction swelling process
D_f	Diffusivity	WR	Ratio of work in case of constant applied pressure to W_{max}
e	Electron charge	ε	Dielectric permittivity of the solvent
G	Gibbs free energy		Ratio of maximum work during swelling to free energy released in one cycle
g	Free energy density (with respect to maximum gel volume)	$\eta_{m/cycle}$	
l_B	Bjerrum length	$\eta_{m/mixing}$	Maximum work divided by free energy released by complete mixing of baths α and β
M	Polymer dry weight	κ	Reciprocal of Debye length
n, N	Total number	π	Osmotic pressure
N_A	Avogadro's number	τ_1	Relaxation time for swelling or deswelling
N_x	Number of effective sites	φ	Polymer volume fraction in gel
p	Mechanical pressure applied to gel	χ	Polymer-solvent interaction parameter

Subscripts

0	Reference state, or beginning of time	ion	Ionic
α	Bath α (causing swelling)	max	Maximum
∞	At equilibrium	mix	Mixing
β	Bath β (causing deswelling)	$mixing$	Complete mixing of baths α and β
b	Bath	$mobile$	Mobile ions in gel
$Coul$	Coulombic	$pack$	Hydrogel packing
f	Net fixed charge or final state	s	Salt
$f-$	Negative fixed charge	$site$	Lattice site
$f+$	Positive fixed charge	$swell$	Hydrogel swelling
g	Gel	t	Time
H^+	Hydrogen ions		

1. Introduction

The salinity difference between two water sources/streams offers great potential for clean, renewable energy production[1,2]. Approximately $0.70 - 0.75$ kWh of free energy is released when 1 m^3 of fresh water flows into the sea[3–5], and the value rises up to 14 kWh if fresh water flows into hyper-saline sources like the Dead Sea[6]. The global salinity gradient power (or osmotic power) is estimated to be $1.4 - 2.7$ TW, which is comparable to the worldwide hydropower capacity (~ 1 TW)[7,8]. The actual potential may be even higher, if other saline sources are taken into consideration, such as brackish water.

Efforts to harvest salinity gradient energy date back to 1954[1], when Pattle described the use of ion exchange membranes to control the mixing of freshwater and saltwater streams. Today, several processes have been established for osmotic energy extraction based on different mixing mechanisms[8]: Ion exchange, osmosis-driven and vapor pressure difference processes. Reverse electrodialysis (RED) is one example of the ion exchange processes[9,10]. It utilizes a stack of anion and cation exchange membranes to modulate the concentration gradient-driven flow of ions, which generates ionic flux and is then converted to electric current through the oxidation-reduction reactions at the electrodes. Capacitive mixing (CapMix) is another ion exchange process that employs capacitive electrodes with or without the presence of ion exchange polymer/membranes[11,12]. Electric charges accumulate at the electrodes when high salinity water is flowed and are discharged when low salinity water is flowed alternatively. Net energy is produced since the energy consumption in charging is less than the energy production in discharging. The most widely studied process is the osmosis-driven pressure retarded osmosis (PRO)[3,13,14]. By placing a semipermeable membrane between two streams of different salinity, water permeates naturally from the lower salinity solution to the higher one. If a hydraulic pressure lower than the osmotic pressure is applied to the high salinity stream, the water permeate flow is retarded and the permeate water is pressurized, which can then drive a hydroturbine to generate electricity. Vapor pressure difference processes utilize the vapor pressure difference between the two solutions with different salinity[15], which is less commonly seen. In fact, all the aforementioned processes for salinity gradient energy extraction can also be divided into membrane-free and membrane-based types. While the former suffers from extremely low energy efficiency, the latter requires the use of large areas of membranes which eventually lead to serious membrane fouling and cleaning concerns[6,16,17], and is typically uneconomical except in applications involving high salinity[18].

Charged hydrogels are a group of polymeric materials that respond to changes in salinity by changing their volume[19–22]. For example, polyelectrolyte hydrogels absorb ions from concentrated salt solution which then shield the electrostatic repulsion between polymer chains[19,21,22]. The gel hence shrinks until the osmotic and elastic effects within the gel are balanced. If the solution is changed to a dilute one, the reverse process occurs and the gel swells. A different trend is observed for polyampholyte hydrogels with balanced or slightly unbalanced charges[20]. The absorption of ions from concentrated solutions shields the electrostatic attraction between opposite fixed charges and leads to gel swelling. There has been increasing interest in recent years to utilize the response of charged hydrogels to salinity for seawater and brackish water desalination[23,24], and osmotic energy extraction via CapMix[25] or coupling with mechanical stress[26–29].

When mechanical stress is applied to the hydrogel to retard its swelling or deswelling, work will be done by the gel that transforms the 'salinity gradient' energy into mechanical energy. This chemo-mechanical coupling in hydrogels is of great importance in this process[30]. Hydrogels may present a good opportunity to exploit the salinity gradient energy, since they can be superhydrophilic and fouling-resistant, which hence reduces the need for cleaning and lowers the operational cost. In 2014, Zhu et al.[26] reported an experimental demonstration of energy extraction from poly (acrylic acid) hydrogels by adding weights on top of the gel, with an energy conversion efficiency of 0.34%. More studies have emerged in the past two years to demonstrate the extraction of osmotic energy via different polyelectrolyte[27,28] or polyzwitterionic hydrogels[29]. The highest energy efficiency reported thus far is ~1.8%[27]. However, all such reports, including those on hydrogels for desalination, are based solely on experimental observations. Little is known about the thermodynamic performance limits of such processes and the engineering principles for the proper design of materials and processes for this kind of energy conversion.

In fact, the swelling and deswelling of gels in aqueous media is not a new topic. Starting from Flory[31,32], numerous studies have been devoted to the understanding of the volumetric response of charged hydrogels to different salt concentrations[20,22,33–35]. However, these are general studies on the swelling phenomenon that do not relate hydrogel swelling to 'salinity gradient' energy conversion. A theoretic framework is indeed highly necessary in the current context, not only to provide overall insights into the potential of energy generation by hydrogels from salinity gradient, but also to give guidelines on the material and process design for future research. In addition, it will also shed light on the exploration of hydrogels for desalination.

In this study, we explore the potential of hydrogels for energy production by thermodynamic analysis and experimental demonstration. The degree of swelling or deswelling within the hydrogel is closely related to its charge properties and elastic modulus. Understanding of the chemo-mechanical coupling in hydrogels first allows us to mathematically model the swelling and deswelling process. Then, a swelling-deswelling cycle is designed where energy is extracted either by an ideal process or by a constant pressure. The total released free energy, maximum energy efficiency and actual efficiency in one swelling cycle is calculated. The design of materials and the effects of salinity are also discussed. In addition, experimental studies are conducted on poly (styrene sulphonate) and poly (sulfobetaine methacrylate) hydrogels as representatives of polyelectrolyte and polyampholyte hydrogels, respectively, to support the theoretical analysis and demonstrate the possibility of energy production by hydrogels from salinity gradients.

2. Theoretical framework
2.1 Swelling equilibrium of hydrogels
2.1.1 Swelling equilibrium and free energy of polyelectrolyte hydrogels
The swelling equilibrium of hydrogels in an external solution bath is achieved when the chemical potentials of each exchangeable species are equal in every phase[32,36]. For polyelectrolyte or polyampholyte hydrogels, the electrochemical potentials of the mobile ions are equal in both the gel and the bath, which is described by Donnan equilibrium.

Similarly, the chemical potentials of the solvent (water) in the two phases are also equal, which can be expressed as follows (eq. (1))[22,33,36,37].

$$\Delta \mu_{g,w} - \Delta \mu_{b,w} = \frac{\partial \Delta G_g}{\partial n_{g,w}} - \frac{\partial \Delta G_b}{\partial n_{b,w}} = 0 \tag{1}$$

where μ is the chemical potential, G is the Gibbs free energy, Δ refers to the difference against reference states as described below, n is the total number (of water molecules in the respective phase), and subscripts g, b and w refer to gel, solution bath and water, respectively.

The total Gibbs free energy of the hydrogel phase has contributions from five different terms: mixing of polymer and solvent (ΔG_{mix}), elastic (ΔG_{el}), ionic (ΔG_{ion}), and Coulombic (ΔG_{coul}) interactions, and pV_g, where p is the pressure difference between the gel and the bath due to an externally applied mechanical force, and V_g is the hydrogel volume. Eq. (2) is obtained as the variation of the five terms have been shown to be mutually independent[22,32,36]:

$$\Delta G_g = \Delta G_{mix} + \Delta G_{el} + \Delta G_{ion} + \Delta G_{coul} + \Delta(pV_g) \tag{2}$$

The free energy of mixing between polymer and solvent is given by the Flory-Huggins' lattice theory, as described in eq. (3) (see Supplemental Material), where R is the gas constant, T is the absolute temperature, v_{site} is the molar volume of lattice site, χ is the polymer-solvent interaction parameter, and φ is the polymer volume fraction in the gel[32]. The reference state is the polymer and solvent before mixing.

$$\Delta G_{mix} = RT \frac{V_g}{v_{site}} (1 - \varphi) \left[\ln(1 - \varphi) + \chi\varphi \right] \tag{3}$$

The elastic energy of the gel under the affine network model is given by eq. (4), which uses the as-synthesized gel status, with the number of effective sites (or monomers) between crosslinks N_x, and the volume fraction of polymer φ_0, as the reference state[22,31,32]:

$$\Delta G_{el} = \frac{3RT}{2} \frac{V_g \varphi}{N_x v_{site}} \left[\left(\frac{\varphi_0}{\varphi} \right)^{2/3} - 1 - \frac{1}{3} \ln \left(\frac{\varphi_0}{\varphi} \right) \right] \tag{4}$$

The term $V_g\varphi/N_x v_{site}$ is the effective number (in mole) of polymeric segments (usually monomers) per crosslink in the network, and φ_0/φ is the swelling ratio. The polymer volume fraction, gel volume and gel diameter or size, D, are related as follows:

$$\frac{\varphi_0}{\varphi} = \frac{V_g}{V_{g,0}} = \left(\frac{D}{D_0} \right)^3 \tag{5}$$

Similarly, the Flory-Rehner theory predicts the elastic modulus, E_m in (eq. (6)) for affine networks[32,38]:

$$E_m = \frac{RT}{N_x v_{site}} \varphi_0 \left(\frac{\varphi_0}{\varphi} \right)^{-1/3} \tag{6}$$

The third contribution comes from the mixing energy between mobile ions and water by considering the ideal gas contribution, as given by eq. (7)[32], which employs the ideal ions and water as the reference state, and assumes dilute ion concentration, *i.e.*, negligible number of mobile ions compared to the total number of water molecules (See Supplemental Material):

$$\mathrm{D}G_{ion} = RTC_{mobile}V_g \ln\left(\frac{C_{mobile}}{C_{mobile} + C_{g,w}}\right) \tag{7}$$

where C_{mobile} is the concentration of all mobile ions in the hydrogel (including H^+ and OH^-), and $C_{g,w}$ is the concentration of water in the gel. In this study, monovalent, fully dissociated NaCl salt is used and all concentrations refer to molar concentrations. The ions partition in such a way so as to ensure electroneutrality, and C_{mobile} is therefore obtained by Donnan equilibrium (Eq. (8), see Supplemental Material for details), which assumes that the entire gel volume is accessible to the ions:

$$C_{mobile} = 2\sqrt{C_b^2 + \left(\frac{C_f}{2}\right)^2} \tag{8}$$

where C_b is the total ion concentration of one sign in the bath (*i.e.*, total cations or total anions), which is related to the salt and proton concentrations in the bath (C_s and C_{H+}, respectively) by $C_b = C_s + C_{H+}$ (assuming monovalent ions and complete salt dissociation). C_f is the net fixed charge concentration in the network. For polyelectrolyte hydrogels, $C_f = f\varphi/v_{site}$, where f is the charge per monomer on the polymer backbones. For polyampholytes, $C_f = |C_{f+} - C_{f-}|$, where C_{f+} and C_{f-} refer to the positive and negative fixed charge concentrations, respectively. To quantify the degree to which salt penetrates into the gels, C_{ratio} is defined in eq. (9) as the concentration of salts that diffuse into the gel over the total concentration of salts in the bath:

$$C_{ratio} \equiv \frac{C_{mobile} - C_f}{2C_b} \tag{9}$$

When the hydrogel completely rejects the salt ions, only counterions are present, giving $C_{mobile} = C_f$ and $C_{ratio} = 0$.

The Coulombic interactions within the gels may be separated into two parts: electrostatic interactions among mobile ions, and those among fixed charges. As the electrostatic interactions among mobile ions can be represented by the activity coefficient and incorporated into eq. (7) (which is eventually neglected as discussed in the Supplemental Material and Fig. S1), contributions from fixed charge interactions are incorporated as represented by eq. (10) (See Supplemental Material for detailed discussion)[39]:

$$\mathrm{D}G_{Coul} = RTl_B \left(fN_x\right)^2 \left(\frac{j}{v_{site}N_x}\right)^{4/3} \frac{V_g}{3^{1/3}}\left[\frac{1}{3}\ln\left(\frac{3v_{site}N_x}{j}\right) - \ln\left(bN_x^{1/2}\right)\right] \tag{10}$$

where l_B is the Bjerrum length, and b is the bond length.

In addition, the Gibbs free energy of the bath solution is given by eq. (11), which represents the ideal energy of mixing of the ions and solvent (*i.e.*, neglecting any Coulombic or enthalpic interactions between ions and the solvent, as is discussed in the Supplemental

Material), assuming a dilute solution (*i.e.*, negligible interaction between ions), and $\varphi \ll 1$:

$$\Delta G_b = 2RTC_b V_b \ln\left(\frac{2C_b}{C_b + C_{b,w}}\right) \tag{11}$$

where $C_{b,w}$ is the water concentration in the bath.

The balance of chemical potentials for water between the gel and the bath is expressed in eq. (12)[32], which is another way to express eq. (1) in terms of the osmotic pressure of water:

$$\Delta \rho_{swell} = \frac{\Delta m_{g,w} - \Delta m_{b,w}}{v_w} = 0 \tag{12}$$

where $\Delta \pi_{swell}$ denotes the potential of the hydrogel to swell in a given salt solution, and v_w is the molar volume of water. Combining eq. (10) with eqs. (1) – (5) and (7) – (9), the condition for equilibrium can be expressed as follows (see Supplemental Material):

$$
\begin{aligned}
&-\frac{RT}{v_{site}}[\ln(1-j) + j + cj^2] + \frac{RTj_0}{N_x v_{site}}[\frac{1}{2}(\frac{j}{j_0}) - (\frac{j}{j_0})^{1/3}] \\
&+ RT(C_{mobile} - 2C_b) \\
&- RTl_B(\frac{j}{3v_{site}N_x})^{4/3}(fN_x)^2[1 - \frac{1}{3}\ln(\frac{3v_{site}N_x}{j}) + \ln(bN_x^{1/2})] \\
&- p = 0
\end{aligned}
\tag{13}
$$

The first two terms represent the osmotic pressure of water in the hydrogel due to the polymer-solvent mixing, and the elastic deformation of the polymer, respectively. The third term $RT(C_{mobile} - 2C_b)$ is the osmotic pressure difference due to the ions in the gel and in the bath for ideal, dilute solutions. The fourth term is the osmotic pressure due to the Coulombic interactions between the polymer chains, whereas the last term is due to the externally imposed pressure on the hydrogel.

Based on eq. (13), one can calculate the polymer volume fraction at given pressure, temperature and solution bath conditions, if the as-synthesized state of the hydrogel is known.

2.1.2 Swelling equilibrium and free energy of polyampholyte hydrogels

The total Gibbs free energy of polyampholyte hydrogels is similar to that in the case of polyelectrolytes, except for the details regarding mobile ion concentration in the gel and the Coulombic interactions among fixed charges, due to the existence of both positive and negative ions in the polymer chains. Eqs. (1) – (8) can then be directly applied to polyampholyte gels.

For polyampholytes whose fixed charge concentrations of both signs are equal or do not differ too much, the electrostatic interactions among fixed charges may be described by a quasilattice model, which gives the free energy as[20]

$$\Delta G_{coul} = -\frac{A}{2}N_{fe}\frac{e^2}{4\rho e}\frac{\exp(-kr)}{r} \tag{14}$$

where $N_{fe} = N_{f+} + N_{f-} - 2|N_{f+} - N_{f-}|$ is the effective number of fixed charges giving rise to attractive interactions, N_{f+} and N_{f-} are the number of positive and negative fixed charges, respectively, A is a parameter in the order of unity similar to the Madelung constant of the ionic crystals (named as quasilattice parameter in this study), e is the electron charge, ε is the dielectric permittivity of the solvent, r is the nearest neighbor distance as given by

$$r \gg 2\left(\frac{3V_g}{4\rho(N_f^+ + N_f^-)}\right)^{1/3}$$

(15)

and κ is reciprocal of Debye length in the hydrogel

$$k = \sqrt{\frac{e^2 N_A^2 C_{mobile} 10^3}{\varepsilon RT}}$$

(16)

where N_A is Avogadro's number. The factor 10^3 is to convert the unit of C_{mobile} from mol L^{-1} to mol m^{-3}.

Combining eq. (12) with eqs. (1) – (5), (7), and (14) – (16) leads to[20]

$$-\frac{RT}{v_{site}}[\ln(1-\varphi) + \varphi + C\varphi^2] + \frac{RT\varphi_0}{N_x v_{site}}[\frac{1}{2}(\frac{\varphi}{\varphi_0}) - (\frac{\varphi}{\varphi_0})^{1/3}]$$

$$+RT(C_{mobile} - 2C_b)$$

$$-\frac{A}{2}\frac{N_{fe}}{V_g}\frac{e^2}{12\rho\varepsilon}\frac{\exp(-kr)}{r} \cdot \{1 + kr - \frac{3kr}{2}[1 + (\frac{2N_A V C_0}{N_{f+} - N_{f-}})^2]^{-1}\}$$

$$-p = 0$$

(17)

through which we can also predict the swelling behavior of a polyampholyte hydrogel in salt solutions at given temperature and pressure.

2.2 Thermodynamic potential of energy production from hydrogel swelling-deswelling cycles
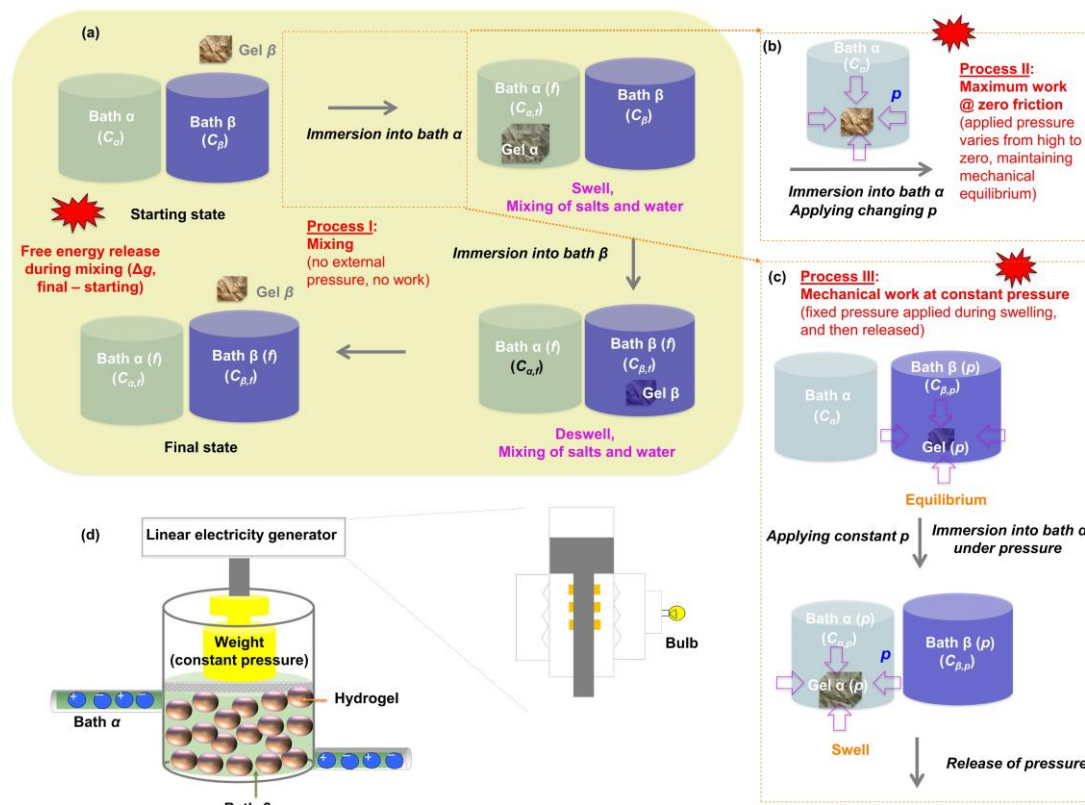### 2.2.1 Release of free energy

Fig. 1 (a-c) Illustrations of thermodynamic cycles for 'salinity gradient' energy conversion using hydrogels. (a) Process I: One swelling-deswelling cycle where a hydrogel immersed sequentially in infinite external baths α and β. The hydrogel starts from state β to represent the gel that has been repeatedly exchanged between the two baths; some mixing occurs in the process. (b) Process II: After immersion into bath α, an external pressure is applied and gradually reduced to zero while maintaining mechanical equilibrium; this zero-frictional swelling process under varying pressure extracts the maximum work for a given hydrogel and baths. (c) Process III: After immersion into bath α, a constant external pressure is applied during swelling. The pressure is released after mechanical equilibrium is reached. (d) An example of electricity generation by a linear generator utilizing the mechanical energy produced through the swelling-deswelling of hydrogels against a 'salinity gradient'. 'C' denotes salt concentration of the baths, subscript 'f' denotes the final states of the gel and bath, and '(p)' denotes states when pressure is applied. The processes are further detailed in Fig. S2 (part A), and illustrations of the p -V_g and $\mu_{g,w}$ -V_g curves in processes I, II and III are in Fig. S2 (part B).

When hydrogels swell or deswell in an external bath, both water and solutes can diffuse in and out of the gel, changing the concentration of solutes in each phase and releasing mixing energy that is initially stored in the solute-solvent system. Meanwhile, energy transformation occurs within the gel; for example, part of the released mixing energy is transformed into elastic energy during the swelling process and the stored elastic energy is

10

later released during the deswelling process. The change in total Gibbs free energy of both phases marks the maximum possible non-expansion work exchange with the surroundings under constant temperature and constant pressure of the gel-bath system[37].

If the salt concentration in the external bath is alternated between high and low concentrations, the hydrogel will undergo swelling and deswelling in response (Process I). In one swelling-deswelling cycle for typical polyelectrolyte hydrogels, as illustrated in Fig. 1a and detailed in Fig. S2 (Process I) the hydrogel is immersed in an external bath α, and swells until it reaches an equilibrium state α. The hydrogel is then immersed in an external bath β with a higher salt concentration than the bath α, and it shrinks until it reaches the equilibrium state β. It is then immersed back into the external bath α, and the cycle repeats. Free energy is released to the environment in the swelling and deswelling processes, and in one swelling/deswelling cycle it is given by eqs. (18), (19) and (20), respectively.

$$\Delta g_{swel} = (\Delta G_{g,a} + \Delta G_{b,a,f} - \Delta G_{g,b} - \Delta G_{b,a})/V_{pack} \qquad (18)$$

$$\Delta g_{deswel} = (\Delta G_{g,b} + \Delta G_{b,b,f} - \Delta G_{g,a} - \Delta G_{b,b})/V_{pack} \qquad (19)$$

$$\Delta g_{cycle} = (\Delta G_{b,a,f} + \Delta G_{b,b,f} - \Delta G_{b,a} - \Delta G_{b,b})/V_{pack} \qquad (20)$$

where Δg_{swel}, Δg_{deswel}, Δg_{cycle} are the released free energy density with respect to the hydrogel packing volume V_{pack}, which is defined as the maximum hydrogel volume, or $V_{g,\alpha}$, in the swelling, deswelling and cyclic processes, respectively. $\Delta G_{g,\alpha}$, $\Delta G_{g,\beta}$, $\Delta G_{b,\alpha}$, $\Delta G_{b,\beta}$ are the free energy of the gel (subscript g) and the bath (subscript b) in the α and β states, respectively. $\Delta G_{b,\alpha,f}$ and $\Delta G_{b,\beta,f}$ refer to the final free energy of bath after mass exchange with the gel. As seen in eq. (20), the net result of one cycle is some mixing of baths α and β, the extent of which depends on the gel, with no net change in the free energy of the gel. Note that the value of released free energy density is negative in sign, but later we express it as its magnitude for ease of discussion. It is also noted that for polyampholyte hydrogels, the salt concentrations of bath α may be higher than bath β.

The Gibbs free energy of the gel and the bath are given by eqs. (2) and (11), respectively. The final ion concentration of the bath in equilibrium with the hydrogel is obtained by applying mass balance over the gel-bath system (see Supplemental Material), while the total volume of the system is assumed constant. The equilibrium state of the system is given by eq. (13) (eq. (17) for polyampholyte hydrogel. With known ion concentrations in each solution, one can calculate the free energy of the system in each state by using the respective equations in Section 2.1.

The energy density may also be calculated with respect to the dry weight M of the polymers within the gel ($\Delta g'$, J g^{-1}) or the total volume of the external baths. In this paper, all energy or work densities are expressed in terms of per packing volume (which is the maximum hydrogel volume as defined earlier), unless otherwise specified.

2.2.2 Maximum extractable work and thermodynamic efficiency

At constant temperature and constant volume of the gel-bath system, the maximum useful work that can be performed by the system on the environment equals the total free energy released by the system when it goes from its initial state to an equilibrium state[37]; this maximum work is performed only when the process is thermodynamically reversible. The process is reversible only if infinitesimal changes are induced to the system so that the

system is always in thermodynamic equilibrium. Two thermodynamic equilibria exist in the gel-bath system – the equilibrium for water and the Donnan equilibrium for salts. As illustrated in Fig. 1(b) and Fig. S2 (Process II), if a pressure is applied to the hydrogel such that it always ensures the swelling or deswelling process is infinitesimally slow, or mathematically the left hand sides of eqs. (13) or (17) are infinitesimally close to zero throughout the process, thermodynamic equilibrium for water can be considered as being maintained (Process II). However, it is not possible to maintain thermodynamic equilibrium for salts and water at the same time, unless there is a semipermeable barrier or an applied electric potential difference that prevents ions from freely diffusing between each phase. Therefore, diffusion of salt ions releases free energy that is not utilizable as mechanical work. Since the permeability of the hydrogel to ions is mainly controlled by its charge density and complete prevention of ion diffusion is hardly realistic in the case of existing hydrogel materials as will be discussed later, a reversible process is not practically attainable by solely applying a mechanical pressure on the hydrogel. For a given hydrogel, to maximize the energy output, one can apply a time-varying pressure that keeps the water in the hydrogel in continuous equilibrium with water in the external bath, so as to avoid frictional loss caused by flow of water in the hydrogel during swelling or deswelling. We define Process II as a zero-frictional process. The maximum extractable work per unit packing volume can be calculated through integration of the applied pressure over the changes in hydrogel volume, dV_g:

$$W_{\max} = \frac{\int_0^{\Delta V_g} p\,dV_g}{V_{pack}} \tag{21}$$

Note that the applied pressure represents a mechanical force applied internally to a part of the system (*i.e.*, the hydrogel), and is not the pressure exerted by the environment on the entire system (hydrogel and bath). Since the process is infinitely slow, it is assumed that after rapid mixing at the beginning, salt is always at equilibrium between the hydrogel and the bath. Throughout the process, the equilibrium volume of the hydrogel is calculated at each value of the applied pressure: the applied pressure changes from an initial value where the water in the gel is in equilibrium with water in the bath at the initial gel volume, to a final value of zero. Since, practically it is easier to capture the energy released in the swelling process, only the work done by swelling is counted and the word *work* hereafter refers to the work extracted in hydrogel swelling (Fig. 1b).

Based on the process described in Section 2.2.1, the thermodynamic efficiencies of Process II are defined as the work extracted during the swelling step ($W_{\max}$) divided by the energy released in the swelling step ($\eta_{m/swell}$) or in the whole cycle ($\eta_{m/cycle}$) as follows:

$$\eta_{m/swell} = \frac{W_{\max}}{\Delta g_{swel}} \times 100\% \tag{22}$$

$$\eta_{m/cycle} = \frac{W_{\max}}{\Delta g_{cycle}} \times 100\% \tag{23}$$

As defined in eqs. (18) and (20), Δg_{swell} and Δg_{cycle} are related to the initial and final (after water and ion exchange with the gel) volume and concentration of baths α and β. For infinite baths, the final volume and concentration of the baths should be only slightly different from their initial states. If the hydrogel completely rejects salts, thermodynamic

equilibrium is maintained throughout the swelling process and $\eta_{m/swell} = 100\%$. Otherwise, $\eta_{m/swell}$ is smaller than 100%.

2.2.3 Work under constant pressure and work ratio

In reality, frictional loss is almost inevitable due to the difficulty in implementing a continuously matching pressure and the need to perform the processes in finite time. It may be more technically feasible to apply a constant pressure in certain systems such as when pressure is exerted by a constant weight. We therefore also consider a Process III involving the application of a constant pressure on the hydrogel as one limiting case, illustrated in Fig. 1c and Fig. S2. The hydrogel in equilibrium with solution β is first squeezed by a constant pressure until a new equilibrium is reached, and then the external bath is changed to solution α in which the hydrogel swells under the same pressure until equilibrated. The gel is finally relaxed to its free state in solution α when the pressure is removed, after which it is allowed to achieve equilibrium and shrink in solution β to return to the initial state. Unlike the zero-friction process with variable pressure, only one pressure is applied in this case. The work done by this constant pressure per unit packing volume is given by

$$W = \frac{p(\Delta V_{g,2} - \Delta V_{g,1})}{V_{pack}} \tag{24}$$

where $\Delta V_{g,1}$ and $\Delta V_{g,2}$ refer to the change in hydrogel volume in steps 1 and 2, respectively. A different process (not discussed here) may also be adopted by omitting step 1 and directly applying pressure to the gel when the external bath is changed from β to α.

It is noted that if the baths are infinite, their concentrations remain almost unchanged after interactions with the gel; and if the baths are finite, their concentrations will be different which can be determined based on equations given in section 2.1.

One may compare this work, performed at a constant applied pressure, with the maximum extractable work during swelling (obtained with varying pressure) using the work ratio WR:

$$WR = \frac{W}{W_{max}} \times 100\% \tag{25}$$

2.3 Swelling kinetics

The swelling of hydrogels in the external bath is described as a collective diffusion of the network polymers and shear relaxation process by Tanaka and coworkers[40,41]. For spherical hydrogels, the diameter of the gel at time t is given by the following equation:

$$D_t = D_\infty + (D_0 - D_\infty)B_1\exp(-t/t_1) \tag{26}$$

where D_t, D_∞ and D_0 are the gel diameters at the beginning, time t and equilibrium states, respectively, B_1 is a numerical factor that depends on the geometry, elasticity and osmolality of the gel, and τ_1 is the relaxation time of the slowest mode in the swelling process. By plotting $\ln[(D_t - D_\infty)/(D_0 - D_\infty)]$ against t, one can obtain τ_1 from the reciprocal of the slope. The diffusivity D_f of the gel in the bath is related to τ_1 and the gel diameter D in the following way:

$$D_f = \frac{D^2}{4t_1} \tag{27}$$

13

3. Materials and methods

3.1 Synthesis of hydrogels

A series of poly (styrene sulphonate sodium salts) (PSS) hydrogels with different monomer concentrations and crosslinking degrees were synthesized by dissolving the monomer sodium 4-vinylbenzenesulfonate (Sigma Aldrich, technical, $\geq$ 90%) and the crosslinker N,N'-methylenenbis(acrylamide) (Sigma Aldrich, 99%) in deionized water at 60°C in an oven. The monomer concentration and number of monomers per chain are given in Table 1 (the crosslinker concentration is calculated by dividing the monomer concentration with the number of monomers per chain). A predetermined volume of 1 M ammonium persulfate (APS) solution as the initiator was then added into the solution so that the final APS molar concentration was 1% of the monomer concentration. After that, the solution was purged by bubbling with argon for 5 min, poured into a rectangular mold, sealed with an aluminum tape and allowed to polymerize for 3 h in the oven at 60 °C.

The poly (sulfobetaine methacrylate) (PSBMA) hydrogels were synthesized with [2-methacryloyloxy)ethyl] dimethyl-(3-sulfopropyl) ammonium hydroxide as the monomer and poly (ethylene glycol) dimethacrylate (PEGDMA, Sigma Aldrich, average M_n 750) as the crosslinker as given in Table 1. The process was similar to that of PSS, but the polymerization was allowed to occur at a temperature of 70°C for 1 h.

To prepare spherical PSS beads, 10 g paraffin oil (Sigma Aldrich) containing 0.005 g Span 80 (Sigma Aldrich) was heated to 60 °C. Beads for energy production demonstration were obtained by adding 4 g of the aqueous monomer solution with the desired amount of monomers, crosslinkers and initiators into the oil bath under stirring. The mixture was purged with argon for 5 min and sealed. The oil bath was kept at 60 °C under continuous stirring for 3 h. Beads for kinetic studies were obtained by purging the oil bath and aqueous monomer solution with argon for 5 min, and then adding < 1 μL of the aqueous monomer solution droplets into the oil bath using a pipette (the diameter of a single bead is controlled by the volume of the solution). The mixture was sealed and kept in a stirring water bath at 60 °C for 3 h.

3.2 Characterization of swelling ratio, compressional mechanical strength and morphology

The as-prepared hydrogels were cut into disks with a diameter of 1.25 cm and thickness of 2 mm for further use. To test the swelling ratio, the gel disks were firstly immersed in 600 mM NaCl solutions (also referred to as seawater) and then in NaCl solutions of different concentrations, each for a few days until no further change in gel diameter was observed. The equilibrium gel diameter was recorded and used for the calculation of swelling ratio. In the meantime, the gels that had been equilibrated in deionized water were dried in the oven at 75 °C until a stable weight was reached. The dried polymer weight was used to calculate the actual monomer concentration.

The compressional mechanical strength of the as-prepared and swollen gels in 10 mM and 600 mM solutions was measured using a universal machine (2 kN load cell; Zwick/Roell Z2.5; see Supplemental Material for more details). The actual number of monomers per

chain was estimated from the measured elastic modulus of as-prepared gels and actual monomer concentrations based on eq. (6), which is a commonly used method to estimate the crosslinking density[32].

The surface morphology of gels was characterized by scanning electron microscopy (SEM) (Tescan SEM Vega3). The gels were freeze-dried prior to SEM characterization.

3.3 Measurement of the swelling kinetics

The swelling kinetics of spherical gel beads were determined by measuring the diameter change using an optical microscope (Nikon Eclipse TE2000-U).

3.4 Demonstration of mechanical energy recovery from hydrogels

A demonstration unit for mechanical energy recovery from hydrogels contained four major components (Fig. S3): a polycarbonate column or tube with 1.905 cm inner diameter and 25 cm total length, two hydrophilic polypropylene porous filters with 90 μm pore size and diameter slightly less than 1.905 cm, and a desirable weight. One of the filters was fixed at the bottom of the tube and the other was combined with a second tube (0.635 cm in diameter and drilled with tiny holes on the wall) to form a frictionless and movable filter. In addition, two holes were drilled at the bottom and on the upper wall of the polycarbonate column to connect with silicone rubber tubes that supply solutions to the unit by a peristaltic pump. Prior to tests, the column was filled with gel that was initially equilibrated in solution α to the maximum height of ~ 17.5 cm. In one swell-deswell (or deswell-swell) cycle, solution β was firstly flowed through the gel from the bottom of the tube, until the height of the gel showed no significant decrease. Then a weight was placed while solution α was flowed through the gel until the height of the gel showed no significant increase.

4. Results and discussion

To investigate the potential of hydrogels for energy conversion from salinity gradients, we first calculate the state of hydrogels in equilibrium with a solution bath (Section 4.1.1). This is followed by calculation of the work performed (with applied pressure) when a hydrogel is immersed alternately between two infinite baths at different salt concentrations (Section 4.1.2). In this case (of infinite baths), the bath concentrations do not change appreciably, and the hydrogel facilitates mixing between the two baths in each cycle as shown in Fig. 1. Since we define the pressure applied to the hydrogel, explicit modeling of the viscous losses within the hydrogel is not necessary – the process is assumed to be mechanically reversible in the case of time-varying pressure (Process II) which represents an ideal case with no viscous losses, and it is irreversible in the case of fixed pressure (Process III) where the loss is governed by the applied pressure and not by the nature of viscous losses in the hydrogels. In Section 4.1.3, we consider the case of finite baths, where the hydrogel is alternately immersed in fresh baths of a fixed volume and concentration. This process results in partial mixing of the two baths at a steady rate per cycle, which is more practical and requires accounting of the mass balance of the salt ions between the gel and bath. Finally, Section 4.2 describes experimental work on energy harvesting using polyelectrolyte and polyampholyte hydrogels.

4.1 Theoretical analysis of the potential of hydrogels for harvesting salinity gradient energy

4.1.1 Equilibrium of hydrogels in infinite baths

To enable theoretical prediction of the equilibrium of hydrogels in external baths, the values for parameters such as v_{site}, v_w, χ, l_B, b, N_x and φ_0 in polyelectrolyte hydrogels were estimated based on their realistic ranges at room temperature (298 K)[20]. Here we employ $v_{site} = 0.19$ m^3 mol^{-1} which is equivalent to the molar volume of typical monomers, $v_w = 0.018$ m^3 mol^{-1}, $\chi = 0.3$ since for good solvents χ is less than 0.5, $l_B = 7$ nm as what it is for water, $b = 0.8$ nm for a typical monomer length. In addition, for the as-synthesized hydrogel, a broad range is considered for monomer concentration, $C_{m,0}$, and number of monomers per chain, N_x, with 1.0 to 3.0 M for the former, and 10 to 200 for the latter. φ_0 is obtained by $\varphi_0 = v_{site} C_{m,0}$. The as-synthesized hydrogel volume $V_{g,0}$ is set as 1 m^3 and the charge per monomer is 1 ($f = 1$) unless otherwise specified. Lastly, the NaCl concentration in the external baths of general practical interest is from 1 mM to 1 M. More specifically, 10 mM and 600 mM are chosen to represent brackish or river water and seawater, respectively, for the swelling-deswelling cycle to extract energy. Since in this range C_s is larger by a few orders of magnitude than C_{H+}, we set C_b equal to C_s. For polyampholyte hydrogels, similar parameters are used, with the exceptions that $v_{site} = 0.23$ m^3 mol^{-1} which is equivalent to the molar volume of typical monomers, $f = 1$ (for each sign of charge) and $A = 0.4$ for typical less-ordered polymers compared to a value of around 1.5 for perfectly ordered ionic crystals[20]. In all discussions, the external baths are assumed infinite in volume (or sufficiently large such that further increase in the volume does not cause appreciable change in the released energy), unless otherwise specified.
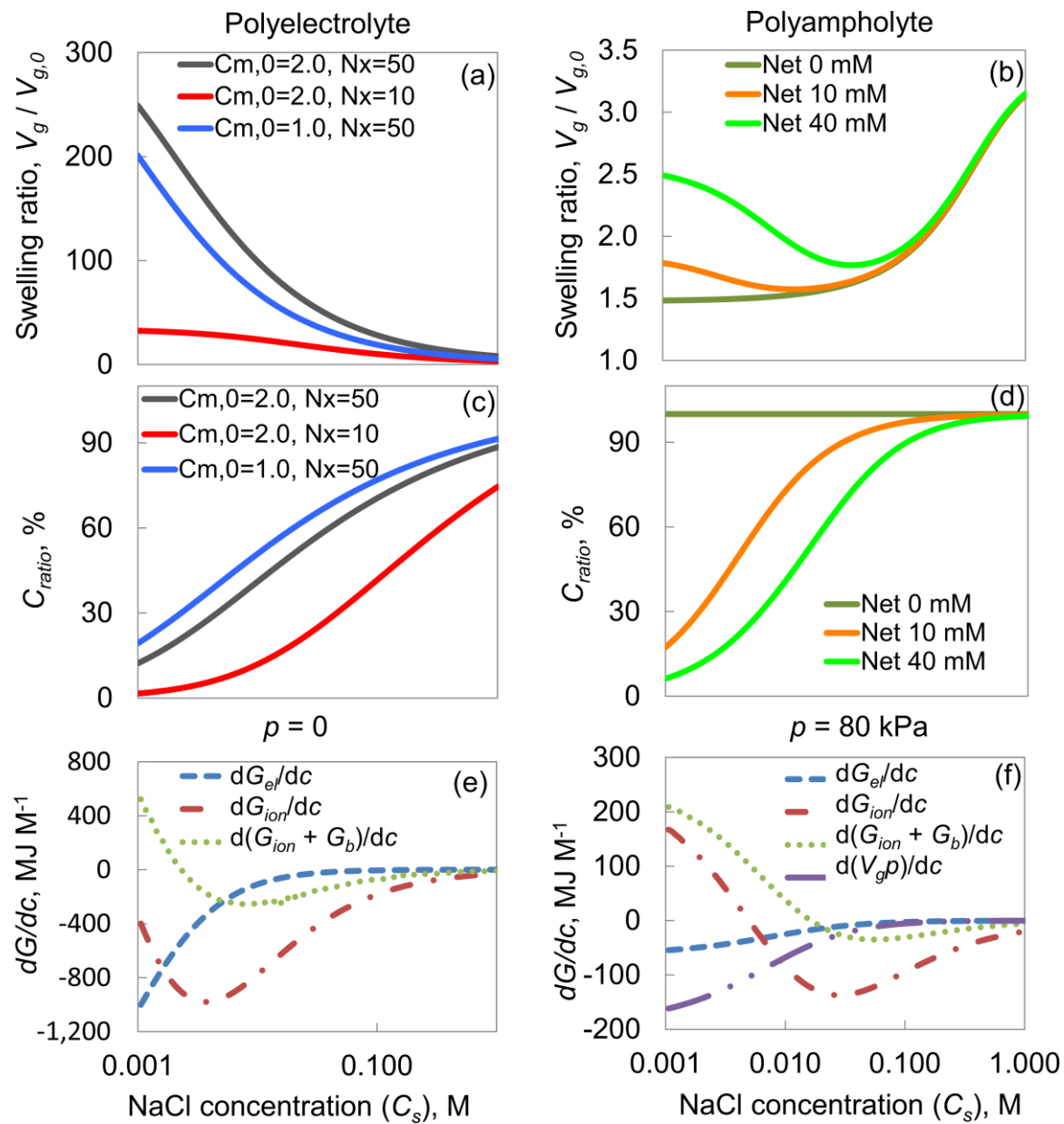
Fig. 2 Theoretical prediction of the effect of NaCl concentration on the hydrogel swelling ratio (a, b) and extent of salt penetration in the gel, C_{ratio}, (c, d) for polyelectrolyte (left) and polyampholyte (right) hydrogels. (e-f) The effect of NaCl concentration on and gel deswelling-induced change indifferent components of free energy expressed as against NaCl concentration (dG/dc), at $p = 0$ (e) and $p = 80$ kPa (f) for a unit volume of the polyelectrolyte hydrogel in its reference state. $d(V_g p)/dc$ in (f) indicates energy conversion to or from mechanical work. $C_{m,0} = 2.0$ M, $N_x = 50$ and $f = 1.0$ in infinite baths were used and $p = 0$ unless otherwise specified in the figure.

Equilibrium hydrogel swelling in an infinite bath. The equilibrium states of hydrogels in NaCl salt solutions at different concentrations, without any external pressure applied on

the gels, are given in Fig. 2. Fig. 2(a) shows that the swelling ratio $V_g/V_{g,0}$ for polyelectrolyte hydrogels decreases upon increasing the salt concentration in the bath due to the screening of repulsion among the fixed charges on the polymer by the salt ions, which is commonly known as the polyelectrolyte effect. In general, the hydrogel swells more at a larger number of monomers per chain, N_x, which corresponds to a lower crosslinking density, and at higher initial monomer concentration $C_{m,0}$, which corresponds to a higher polymer volume fraction. On the contrary, a different pattern is observed for polyampholyte hydrogels, as shown in Fig. 2(b). With equal numbers of opposite charges in the network, the polyampholyte hydrogel swells with increasing salt concentration in the bath, since the attractive forces between opposite charges in the polymer chains are screened by the salts and hence the polymer network opens up. Nonetheless, if the polyampholyte hydrogel has a net charge, it first shrinks with increasing salt concentration at low NaCl concentrations due to screening of the electrostatic repulsion like a polyelectrolyte hydrogel; however, at higher salt concentrations, it swells with increasing salt concentration like a charge-neutral polyampholyte hydrogel and thus exhibits a minimum in volume at an intermediate salt concentration. An interesting observation is that polyampholyte hydrogels swell to a smaller extent than polyelectrolyte hydrogels even at similar monomer concentration and crosslinking degree, indicating that the net charge and hence the free counterions inside the network play dominant roles in hydrogel swelling.

Salt penetration under equilibrium. Meanwhile, the salt penetration ratio (C_{ratio}) defined in eq. (9) is always greater than zero, which shows that both hydrogels do not reject salts completely (Figs. 2(c) and 2(d)). In fact, the net fixed charge on the polymer chains acts as a barrier to prevent salt inflow, according to Donnan equilibrium. The efficiency of rejection depends on the concentration of net charge inside the gel. Salts diffuse to a lesser extent into the gel at higher monomer concentration and crosslinking degree, since the former directly brings more charges into the network and the latter maintains higher charge density by reducing the swollen volume of hydrogels. It is also noted that, for polyampholyte hydrogels with no net charge, Donnan equilibrium predicts that the salt concentrations are equal inside and outside of the gels ($C_f = 0$ and $C_{mobile} = 2C_s$, which gives $C_{ratio} = 1$).

Effect of salt concentration on free energy. The different components of the free energy of hydrogels - mixing, elastic, ionic and Coulombic free energies - vary when the salt concentration of the infinite bath is changed (Figs. S4a and S4b). Furthermore, the swelling or deswelling that accompanies any change in the bath salt concentration has a small effect on the free energy of the bath, and this change in free energy is small in comparison to the change in free energy of the hydrogel (Figs. S4c and S4d, Supplemental Materials). In the case of polyelectrolyte gels, there is almost no net exchange of ions between the gel and the bath at low bath solution salt concentrations (Fig. S4d), and the change in the bath free energy with salt concentration as induced by swelling or deswelling of hydrogels is mainly due to shrinking of the hydrogel. At high NaCl concentration, the change in free energy of the bath in response to the swelling of polyampholyte gels is comparatively high due to the nearly complete penetration of salt in the polyampholyte gel.

18

Fig. 2(e-f) shows the rate at which the different components of the hydrogel free energy vary with salt concentration of the bath. dG_{el}/dc denotes the change in elastic free energy of the gel per unit change in salt concentration of the bath. dG_{ion}/dc and $d(G_{ion}+G_b)/dc$ denote the change in the ionic component of free energy induced by swelling or deswelling in the hydrogel and in the hydrogel plus bath, respectively; the latter represents free energy change due to redistribution of ions between the bath and gel. $d(V_g p)/dc$ represents the mechanical work exchange with the agent applying the external pressure, per unit change in bath salt concentration. The elastic free energy of the hydrogels varies rapidly with salt concentration at low salt concentrations demonstrating a strong coupling between chemical and mechanical energy, but it does not change appreciably at high salt concentrations since deswelling is nearly complete and the chemo-mechanical coupling is much weaker (Fig. 2e,f). Therefore, when external pressure is applied, the mechanical work per unit change in salt concentration is high for dilute solutions and decreases at high salt concentrations (Fig. 2f) where the effect of salt concentration on the hydrogel volume is minimal (Fig. 2a).
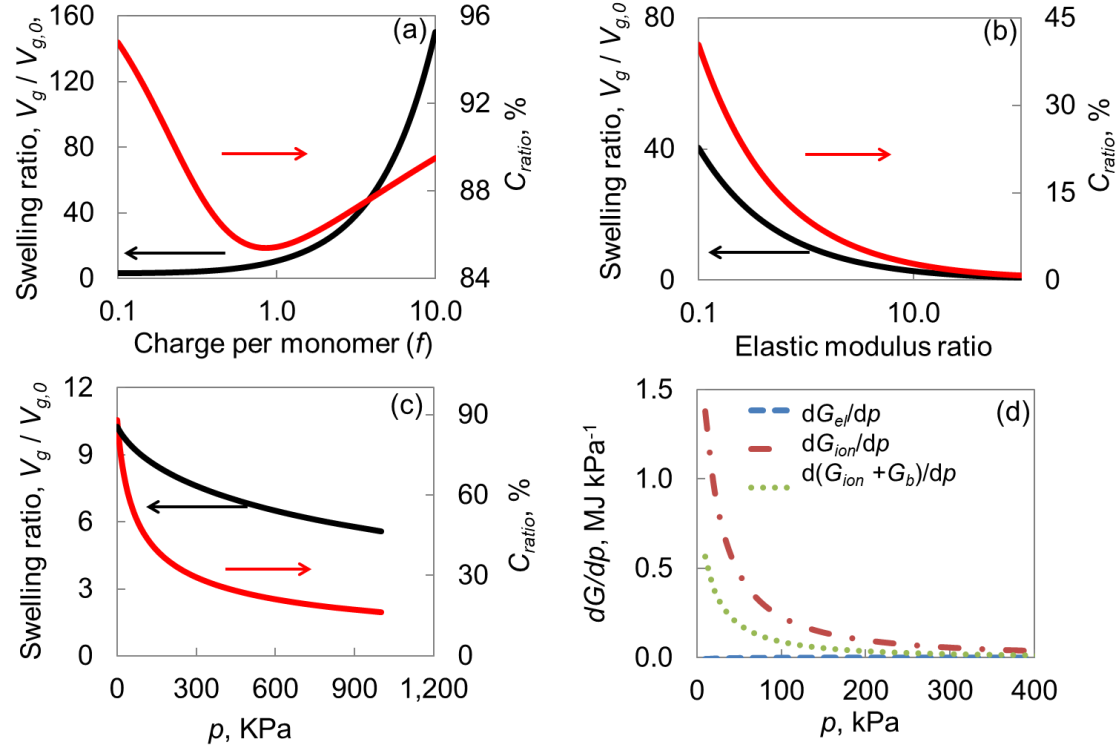
Fig. 3 Theoretical prediction of the swelling ratio and C_{ratio} of polyelectrolyte hydrogels against (a) different charge per monomer, (b) elastic modulus ratio over the original value given by eq. (6), (c) applied pressure difference, and (d) change in free energy (dG/dp) against applied pressure difference. $C_{m,0} = 2.0$ M, $N_x = 50$ and $f = 1.0$ in infinite seawater baths are used and $p = 0$ unless otherwise specified. The values for elastic modulus in the horizontal axis in (b) indicate the relative increase in the elastic modulus achieved by external methods such as implantation of a strong backbone into the network, and are directly added to eq. (13) as a multiplying factor to calculate the corresponding swelling

ratios. Red and black curves are paired with arrows of the same color to indicate the corresponding vertical axis.
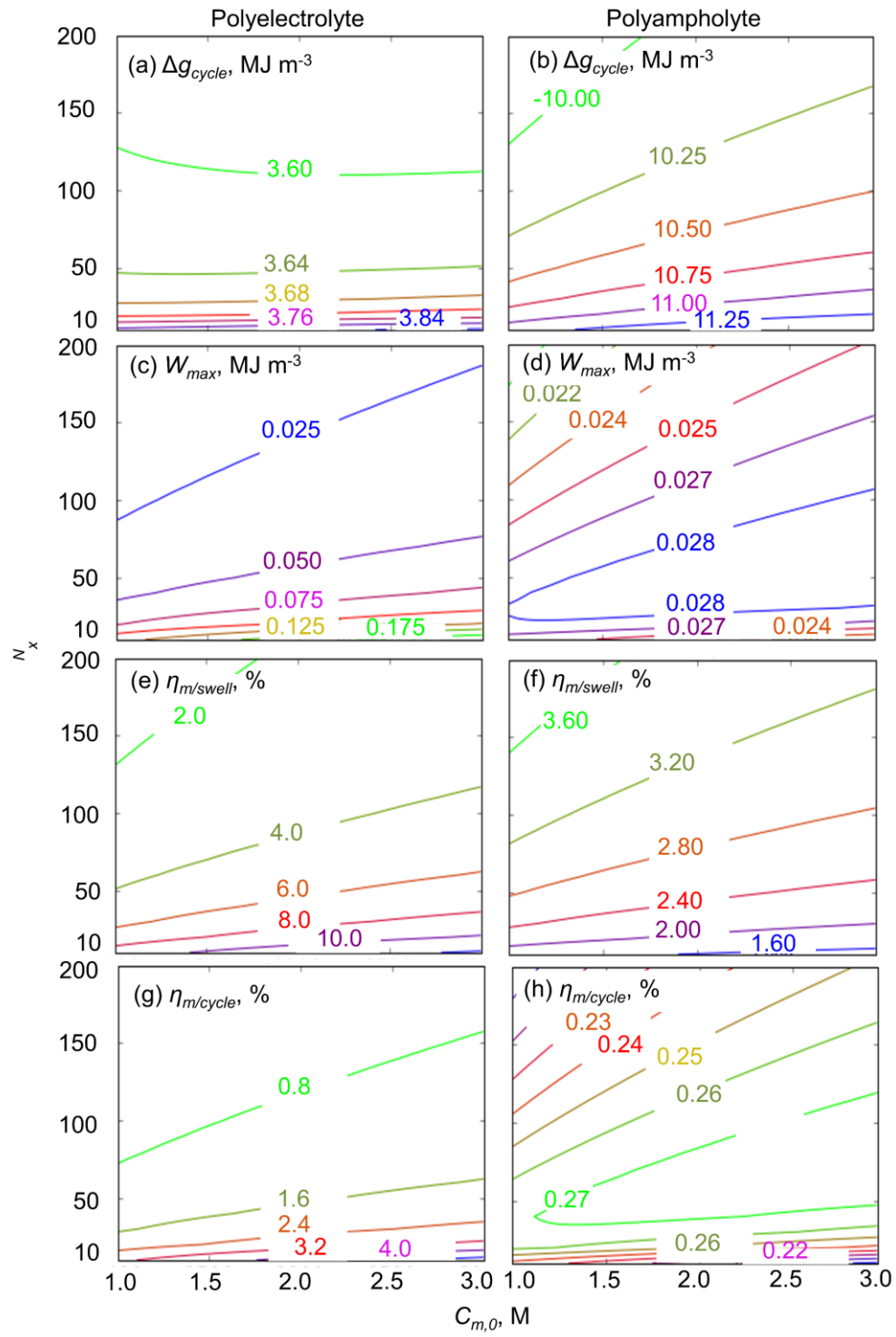
Fig. 4 Theoretical prediction of the (a, b) total released free energy in one swell-deswell cycle, (c, d) the maximum extractable work W_{max} per unit packing volume in the zero-frictional swelling process, (e, f) ratio (%) of W_{max} to the free energy released during swelling ($\eta_{m/swell}$) and (g, h) ratio (%) of W_{max} to the total free energy released in one cycle ($\eta_{m/cycle}$) for polyelectrolyte (left panel, a, c, e, g) and polyampholyte (right panel, b, d, f, h) hydrogels. The external baths are infinite with concentrations of 10 mM and 600 mM NaCl (seawater) respectively. Net charge is 0 mM for polyampholytes.

Effect of charge, elastic modulus, and external pressure on swelling. However, the equilibrium states of hydrogels are changed if the number of charges per monomer (*f*) or the elastic modulus of the hydrogels are varied, or if an external pressure is applied to the hydrogel, as represented by polyelectrolyte hydrogels in seawater in Fig. 3. Increasing *f* from 0.1 to 10.0 directly adds more charges into the network, but also leads to a drastic increase in the swelling ratio, especially when *f* is larger than 1.0 (Fig. 3a). As a result of the competition between Coulombic and elastic effects, the fixed charge concentration and hence the salt penetration ratio (C_{ratio}) first increases and then decreases as the charge per monomer is increased. In the meantime, though elastic modulus is determined by the crosslinking density and polymer concentration within the hydrogel according to eq. (6), it might be greatly enhanced by introducing a second network structure into the gel, as is reported in literature[42,43]. Fig. 3(b) shows that an increase in the elastic modulus results in simultaneous reduction in swelling ratio and salt penetration.

Applying an external pressure on the hydrogels shrinks the hydrogel volume, elevates the fixed charge concentration and reduces C_{ratio} (Fig. 3(c)). Therefore, the elastic free energy decreases while the ionic free energy is greatly increased by the applied pressure. It is found in Fig. 3d and Fig. S4 that the applied pressure induces more significant changes in the free energy of gels at dilute salt concentrations, indicating that a greater fraction of the free energy can be converted into mechanical work at lower salt concentrations under the given external pressure.

4.1.2 Energy conversion and thermodynamic efficiency in infinite baths
Maximum work and efficiency. The potential of energy production by polyelectrolyte hydrogels in infinite NaCl baths is first studied. In one swelling-deswelling cycle (Fig. 1a) using 10 mM and 600 mM NaCl as solutions *α* and *β* respectively to generate the salinity gradient, the free energy density per packing volume that is released from the whole cycle reaches about – 3.6 to –3.9 MJ m^{-3} in the specified $C_{m,0}$ and N_x ranges, as shown in Fig. 4(a). To extract energy from the swelling process to the maximum extent, a zero-frictional process is assumed, where an external pressure is continuously changed so that water in the hydrogel is always in equilibrium with that in the solution (Fig. 1b). Fig. 4(c) shows that ∼ 0.025 to 0.175 MJ m^{-3} of work can be harvested by the process. The thermodynamic efficiency in terms of the ratio of the maximum work over the released energy in the swelling process alone reveals that 2 to 10% of the released energy is converted into work (Fig. 4e). It is also noted that higher efficiency is achieved at a larger monomer concentration and a smaller N_x. The loss in efficiency mainly results from the mutual diffusion of salts between the gel and the solution. The incomplete rejection of salts by the

21

gel (Fig. 2c) makes the mixing process thermodynamically irreversible, and consequently reduces the energy efficiency. In addition, the thermodynamic efficiency in terms of the maximum work divided by the total released free energy in the whole cycle is given in Fig. 4(g) and approaches 4% in the specified range of parameter values.

Apart from $C_{m,0}$ and N_x, the number of charges per monomer and elastic modulus also influence the thermodynamic efficiency, since both affect C_{ratio}, as is discussed earlier. Fig. S5 shows that a higher efficiency is achieved at a reasonably larger number of charges per monomer and better mechanical strength, but the effects of further improvement in strength are less significant. The efficiency decreases if the number of charges per monomer is too large, since the extensive swelling leads to lower charge concentration, as discussed earlier in Section 4.1.1.

For comparison, the thermodynamic efficiency of polyampholyte hydrogels is also studied. Hydrogels with equal numbers of opposite charges are chosen since their volume increases by the largest degree when moved from 10 mM to 600 mM NaCl solutions. Around 10 MJ m^{-3} free energy is released in the swell-deswell cycle (Fig. 4b), which is significantly higher than that for polyelectrolytes. Fig. 2(d) shows that the equilibrium concentration of ions is equal inside and outside of the gel. In other words, the gel does not function as an ion barrier. The salt penetration ratio is the highest among all charged hydrogels, which leads to more significant change in entropy and hence releases a lot of free energy. Nonetheless, in most cases, the maximum work and energy efficiency (Figs. 4d, 4f and 4h) are significantly lower than those in the case of polyelectrolyte hydrogels because the volume change in polyampholyte gels is typically smaller, *i.e.*, the polyampholyte hydrogel simply facilitates mixing of the two solutions with little coupling to mechanical work. Interestingly, higher efficiency is achieved at lower monomer concentrations and especially at lower crosslinking degree (or larger N_x), mainly due to the very limited degree of swelling at high crosslinking density. The results show that polyelectrolyte hydrogels are better candidates for energy production from salinity gradients.
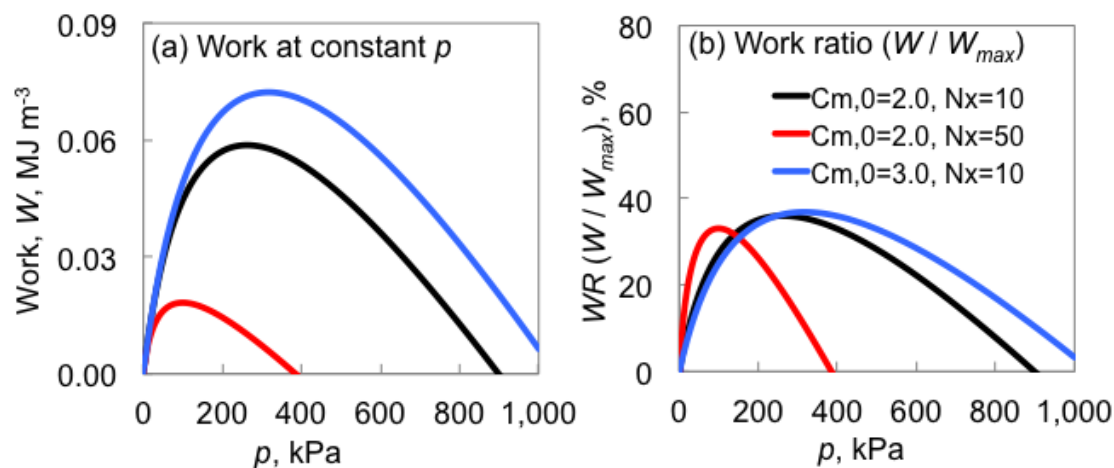
Fig. 5 Theoretical prediction of (a) the work (W) done per unit packing volume in the swelling process under a constant pressure process and (b) ratio (%) of W in a constant pressure process to the maximum extractable work (W_{max}) during swelling ($f = 1.0$). The external baths are infinite.

Work at constant applied pressure. We now consider the constant pressure process as illustrated in Fig. 1c: the gel is first compressed in solution β by pressure, and then it does work on the surroundings (*i.e.*, on the agent applying the external pressure) as it swells in solution α against the applied pressure. Finally, the pressure is released and the compressed gel in solution α relaxes to the equilibrium state at zero external pressure. One practical approach to extract energy from salinity gradient could be applying a constant weight on the hydrogel packed in a piston-cylinder assembly[26–29], which may be connected to a linear electricity generator (Fig. 1d).

It is noted that the energy consumed in the first step for compression was subtracted from the expansion work to obtain the total work; it was also assumed that the energy released in the last step is not utilized to produce work. Meanwhile, some energy is lost due to the friction loss when water passes through gel, since the external pressure does not maintain equilibrium of water between the gel and the solution. Overall, there exists an optimum pressure that maximizes energy production for such a process, since a lower pressure fails to fully exploit the potential work that the gel can do, but a higher pressure wastes too much energy in compressing the gel and also limits the extent of swelling and therefore the work done in the swelling process. The effect of different monomer concentrations and crosslinking degrees on the work extracted under constant pressure (Fig. 5) precisely depicts an increasing and then a decreasing trend as the applied pressure is increased. The optimum pressure ranges from tens to hundreds of kPa. The optimum work ratio, defined as the ratio of work under constant pressure over maximum extractable work in the zero-frictional process (eq. (25)), varies between 30% to 40%, due to the aforementioned loss in compression, friction and non-utilized energy. It is therefore not surprising to see an increasing work ratio from 30.9% to 34.7% when N_x is decreased from 200 to 10 (at $C_{m,0} = 2.0$ M), due to the enhanced elastic modulus at higher crosslinking degree or smaller N_x (eq. (6)).

Effect of salinity on energy efficiency. So far, seawater and brackish water as represented by 600 and 10 mM NaCl solutions are employed. Real applications might involve sources with diverse salinities. To understand the effects of salinity on energy production, the maximum work per packing volume during zero-frictional swelling and its ratio over the total released energy in the full cycle, *i.e.*, the thermodynamic efficiency, is plotted against NaCl concentration (Fig. 6). It is seen that, for a given solution α (10 mM NaCl), a higher salt concentration in the bath β results in higher maximum work per packing volume but a lower efficiency, since the gel continues to deswell in concentrated solutions (therefore leading to more volume change) and yet the degree of deswelling gradually levels off as depicted in Fig. 2a. Meanwhile, if the solution β is fixed at 600 mM NaCl, both maximum work and efficiency tend to increase with decreasing salt concentration of bath α, except at very dilute concentrations, where the mechanical strength of the gel becomes very weak

upon extensive swelling. Overall, lower salinity gives higher thermodynamic efficiency, since the hydrogel is more effective in rejecting salts at lower salt concentrations.
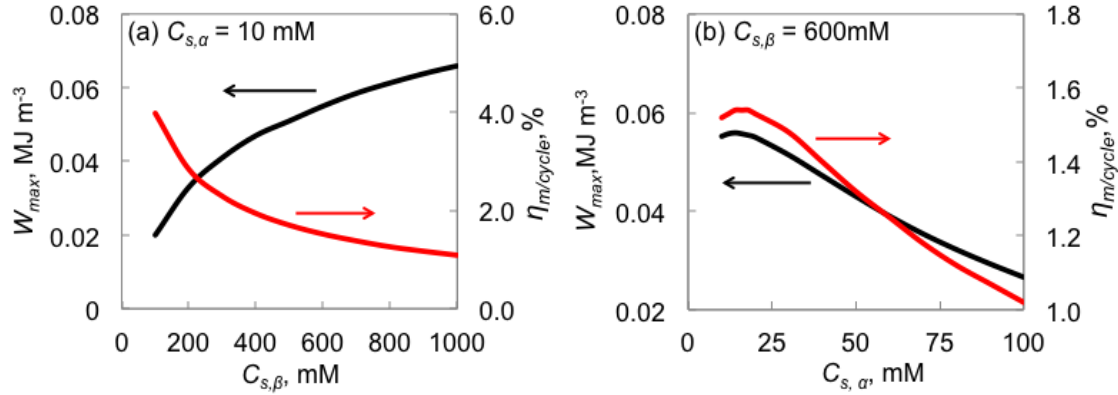

Fig. 6 Theoretical analysis of the effects of NaCl concentration of the other bath on the work in zero-frictional swelling process per unit packing volume (W_{max}) and the ratio of the work in zero-frictional swelling process to the total released energy ($\eta_{m/cycle} = W_{max}/\Delta g_{cycle}$) for (a) bath α concentration of 10 mM NaCl and (b) bath β concentration of 600 mM NaCl at $C_{m,0} = 2.0$ M, $N_x = 50$ and $f = 1.0$. The external baths are infinite. Red and black curves are paired with arrows of the same color to indicate the corresponding vertical axis.

4.1.3 Thermodynamic efficiency in finite baths and potential of hydrogels for osmotic energy production

Energy conversion with finite baths. In real applications, it is hardly possible to implement infinite baths. Therefore, we consider energy extraction from finite baths. One approach to implement such a process is as follows: firstly the hydrogel which is pre-equilibrated in a sufficiently large solution α, is immersed in the external bath β with the volume $V_{b,\beta}$ until it reaches equilibrium, and then it is immersed in the external bath α with the volume $V_{b,\alpha}$ until equilibrium to complete a cycle, similar to that in Fig. 1a but with finite baths. The steps are repeated with fresh baths and a cyclic process is reached after a few iterations (cyclic Processes I-c, II-c, and III-c, as detailed in Figure S2). Mass balance between the gel and the bath is applied (see Supplemental Material) in combination with eqns. (8) and (13) to calculate the concentration of ions in both phases.

Fig. S7A gives representative swelling ratios of the polyelectrolyte hydrogels in 10 mM and 600 mM NaCl solutions (baths α and β, respectively) alternatively as functions of the iterations ($C_{m,0} = 2.0$ M, $N_x = 50$, $f = 1.0$ and $5E_m$). It shows that the swelling ratios in respective solutions quickly reach steady state values within a few iterations. A larger external bath volume of solution α ($V_{b,\alpha}/V_{g,0}$) favors higher swelling ratios, while a larger $V_{b,\beta}$ favors a smaller swelling ratios. It is therefore expected that more work is done when the volume of bath β is larger. The thermodynamic efficiency $\eta_{m/cycle}$, defined as the ratio

of the maximum work in the ideal swelling process to the total released energy in one steady-state cycle (as is defined in eq. (22)) is displayed in Fig. 7a. It is observed that the volume of the dilute bath α has a more prominent effect on the thermodynamic efficiency compared to the concentrated bath β, which is explained by the more sensitive response of gel volume to dilute salt solutions. In general, a larger bath α and a smaller bath β are preferred to achieve higher efficiency. Further increasing $V_{b,\alpha}$ to close to infinity while maintaining a small bath $V_{b,\beta}$ leads to a thermodynamic efficiency of up 5.5% (Fig. S7B). This is higher than the 4.25% efficiency when both baths are infinite, again due to the less sensitive response of gel swelling in the concentrated bath.

Thus far, the thermodynamic efficiency is defined as the work performed compared to the maximum work that can be extracted for the extent of mixing that is achieved in the cycle. The concentrations of baths α and β in their final states (after interacting with hydrogels) are different than the average of the two concentrations, as shown in Fig. S8. In other words, the mixing of both solutions is incomplete. One important concern is hence what the efficiency is if the complete mixing of solutions is assumed. We hereby define a new efficiency $\eta_{m/mixing}$, which is the ratio of the maximum work performed during swelling to the total free energy released if baths α and β mix completely (Δg_{mixing}):

$$\eta_{m/mixing} = \frac{W_{max}}{\Delta g_{mixing}} \times 100\% \tag{30}$$

Fig. 7b suggests that at a small volume of bath β (600 mM) and an optimum volume of bath α (10 mM), the efficiency may go up to 4.2%. In addition, it is reasonable to expect a higher efficiency if the salinity of the concentrated solution is lower as discussed earlier. Alternatively, for given volumes of baths α and β, efficiency may be increased by performing the mixing process in multiple steps or in a staged manner such that the salt concentrations in both baths are gradually brought to the same value, *i.e.*, to complete mixing.
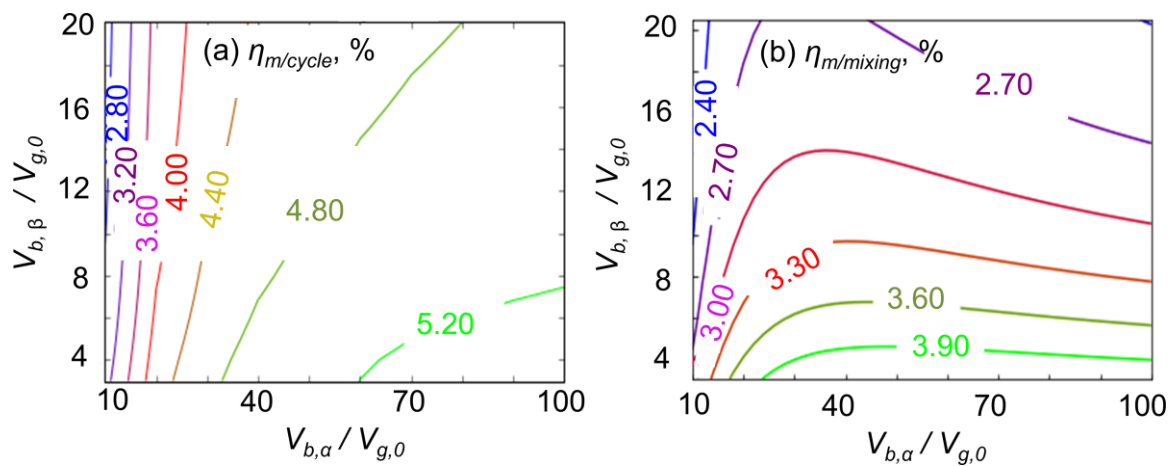

Fig. 7 (a) The maximum work in the ideal swelling process normalized by the total released energy in one cycle ($\eta_{m/cycle}$) and (b) the maximum work in the swelling process normalized

by the total free energy released upon complete mixing of the bath solutions in one cycle ($\eta_{m/mixing}$) for polyelectrolyte hydrogels in the case of fixed, finite volume NaCl baths α (10 mM) and β (600 mM). The analysis is performed at $C_{m,0} = 2.0$ M, $N_x = 50$, $f = 1.0$ and $5E_m$.

It should also be noted that all discussions in this work only convert the energy in the swelling process into work; it is assumed that the energy released in the deswelling process remains completely untapped. If a proper mechanical process is designed so that energy in both swelling and deswelling processed is harvested, one can expect the thermodynamic efficiency to be potentially doubled. Practically, work during deswelling could be captured by approaches such as using composite materials comprising hydrogels embedded in a matrix such as a porous elastic material that can apply tension on the hydrogel.

Overall, as revealed by theoretical analysis, one can molecularly design the hydrogel material with regards to monomer concentration, crosslinking density, charge properties and elastic modulus, carefully select the salinity sources, and at the same time engineer the process to maximize the thermodynamic efficiency and energy output. With proper design, the performance of such hydrogel-mechanical coupling systems may approach that of PRO processes, while offering potential benefits such as ease of manufacture, lower fouling propensity, and ease of cleaning. In particular, hydrogels may be able to effectively harvest the energy of mixing from low salinity streams, and may prove to be more scalable and cost-effective than PRO. However, development of specific designs, further advances in materials, and further analysis will be required to assess the techno-economic feasibility of this approach. We also note that several assumptions have been made in our analysis, as stated in the theory section. The effect of multivalent ions and the behaviors of other kinds of materials beyond hydrogels have not been considered in this work. We now turn to experimental demonstration of the theoretical predictions.

4.2 Experimental demonstration

The foregoing theoretical analysis suggests that polyelectrolyte hydrogels with a high charge density and high crosslinking density (small N_x) are desirable for energy conversion from salinity gradients. Secondly, theory shows that, for a fixed applied pressure, the efficiency increases with pressure and is maximized at an optimal pressure; this pressure is in the 100 kPa range and is practically limited by mechanical failure of the hydrogel due to non-isotropic stresses generated in the application of pressure. Thirdly, the analysis shows that the net amount of work done is insensitive to the salt concentration of the dilute solution, and increases with the salt concentration of the high-salinity solution with a concomitant decrease in efficiency.

First, we systematically varied the monomer and crosslinker concentration to prepare polyelectrolyte and polyampholyte hydrogels with a range of properties. We compared the swelling/de-swelling behavior trends with theoretical predictions, since this behavior determines the overall performance in energy conversion and can guide selection of the polymer for high energy conversion efficiency. The resulting hydrogels were characterized and their properties were compared to theoretically predicted trends, as discussed in the following sections. Based on this characterization, one of the polyelectrolyte hydrogels was

selected to illustrate a proof-of-concept salinity-to-mechanical energy conversion and to quantify the resulting efficiency.

4.2.1 Swelling ratio and mechanical strength of PSS and PSBMA hydrogels

Hydrogel swelling. To experimentally demonstrate the osmotic energy production by hydrogels, PSS, whose fractional charge number is among the highest in all existing polymers (~1), is chosen as a representative polyelectrolyte based on theoretical predictions. Zwitterionic PSBMA (with a slight net negative charge, see Supplemental Material) is used to represent polyampholytes.

Table 1 Initial and actual monomer concentration ($C_{m,0}$), number of monomers per chain (N_x) and charge per monomer f of PSS and PSBMA hydrogels. The initial values are obtained from the pre-gel solution preparation. The actual $C_{m,0}$ is estimated from product yield and the actual N_x is calculated from the elastic modulus of as-synthesized gels based on eq. (6).

Hydrogel	$C_{m,0}$, initial (M)	N_x, initial	$C_{m,0}$, actual (M)	N_x, actual
		PSS		
C1.2-N13	1.2	13	0.9	109
C1.5-N13	1.5	13	1.3	63
C1.8-N13	1.8	13	1.6	30
C1.8-N17	1.8	17	1.6	78
C1.8-N25	1.8	25	1.5	160
		PSBMA		
C1.0-N143	1.0	143	0.8	239
C0.8-N143	0.8	143	0.6	251
C0.6-N143	0.6	143	0.4	704
C0.6-N48	0.6	48	0.5	318
C0.6-N14	0.6	14	0.5	149

Figs. 8(a) and 8(b) prove experimentally that, despite of the large range of $C_{m,0}$ and N_x (specifications of the different hydrogels are given in Table 1), both PSS hydrogel, which is polyelectrolyte, and PSBMA hydrogel, which is polyampholyte with a slight excess of negative charges, show swelling trends consistent with theoretical predictions when placed in NaCl solutions (Figs. 2(a) and 2(b)). In addition, the magnitude of the swelling ratio for PSBMA matches well with predicted values as depicted in Fig. S8a. However, it is interesting to observe that PSS hydrogels swell far less than predicted at low salt concentrations (Fig. S8b), and the slope of the curve for PSS hydrogel swelling at dilute salt concentrations is not as sharp as the theoretical one for reasons discussed below.

Elastic modulus. Representative stress-strain curves of the PSS and PSBMA hydrogels in the as-prepared, 10 mM, and 600 mM NaCl states, which are typical of hydrogels, are displayed in Fig. S9 (a) and S9(b). It is noticed from Fig. S9(c) and S9(d) that the reduced stress of both hydrogels mostly increases at higher strain, which deviates from the Flory-Huggins theory, suggesting that the chain stiffening occurs at higher strains, which may be beneficial for energy harvesting. In addition, the elastic modulus obtained from these curves is plotted in Figs. 8(c) and 8(d). It is seen that as-prepared hydrogels with higher crosslinking density and higher monomer concentration exhibit larger elastic modulus. This is in agreement with the theoretical prediction by eq. (6), where elastic modulus is shown to be positively correlated to the polymer volume fraction and inversely proportional to the number of monomers per chain. The actual crosslinking density is also calculated from the elastic modulus and actual monomer concentration of the as-prepared hydrogels as presented in Table 1. With these values, we can predict the elastic modulus of the gels swollen in 10 mM and 600 mM (or seawater) NaCl solutions, respectively (solid lines in Figs. 8(c) and 8(d)). It is seen that the experimental data of PSBMA hydrogels roughly match theoretical predictions, although there is some discrepancy in exact values that might arise from the deviation from the Gaussian-chain assumption and the contributions of counterions[35]. The elastic modulus decreases at a higher swelling ratio or lower polymer volume fraction.

Anomalous stiffening of PSS hydrogels. However, significant deviation from theoretical prediction occurs in the case of PSS hydrogels; the elastic modulus is much lower than that expected in 600 mM NaCl. Factors such as the degree of ionization and Debye-Hückel screening effects might contribute to the phenomena[34]. On the contrary, when hydrogels swell further in 10 mM NaCl, the elastic modulus not only far exceeds theoretical values, but is also larger than that in 600 mM NaCl. Similar phenomenon has been observed for polyacrylate gels in literature, but only with a slight increase in elastic modulus at extremely high swelling ratio[44]. The discrepancy between theoretical predictions and experiments may arise from the large deformations of the polymer chains in highly swollen states resulting in enhanced stiffness[32], whereas eq. (6) is valid only for relatively small deformations.

The SEM images of the surface morphology of PSS hydrogels in Fig. 8(e) are consistent with this picture. While as-prepared and seawater-swollen hydrogels present more round, porous structures with polymer chains mainly randomly distributed, the 10 mM-swollen gel shows long, fibrous chains. This is possibly because the extensive swelling in dilute solutions induces chain alignment in the network, resulting in a larger elastic modulus. This also explains the limited swelling ratio and the mild slope of swelling ratio against salt concentration at dilute salt solutions in Fig. 8(a), as swelling is inhibited by the large elastic modulus (eq. (11)). In addition, the local entrapment of counterions that causes osmotic passivity in highly charged polyelectrolytes may also partially explain the lower swelling ratio compared to theoretical predictions[45].

The unique mechanical properties of PSS hydrogels make them good candidates for osmotic energy production, since the larger elastic modulus in dilute solutions ensures

excellent anti-compressibility in the swelling process and therefore maximizes work output.
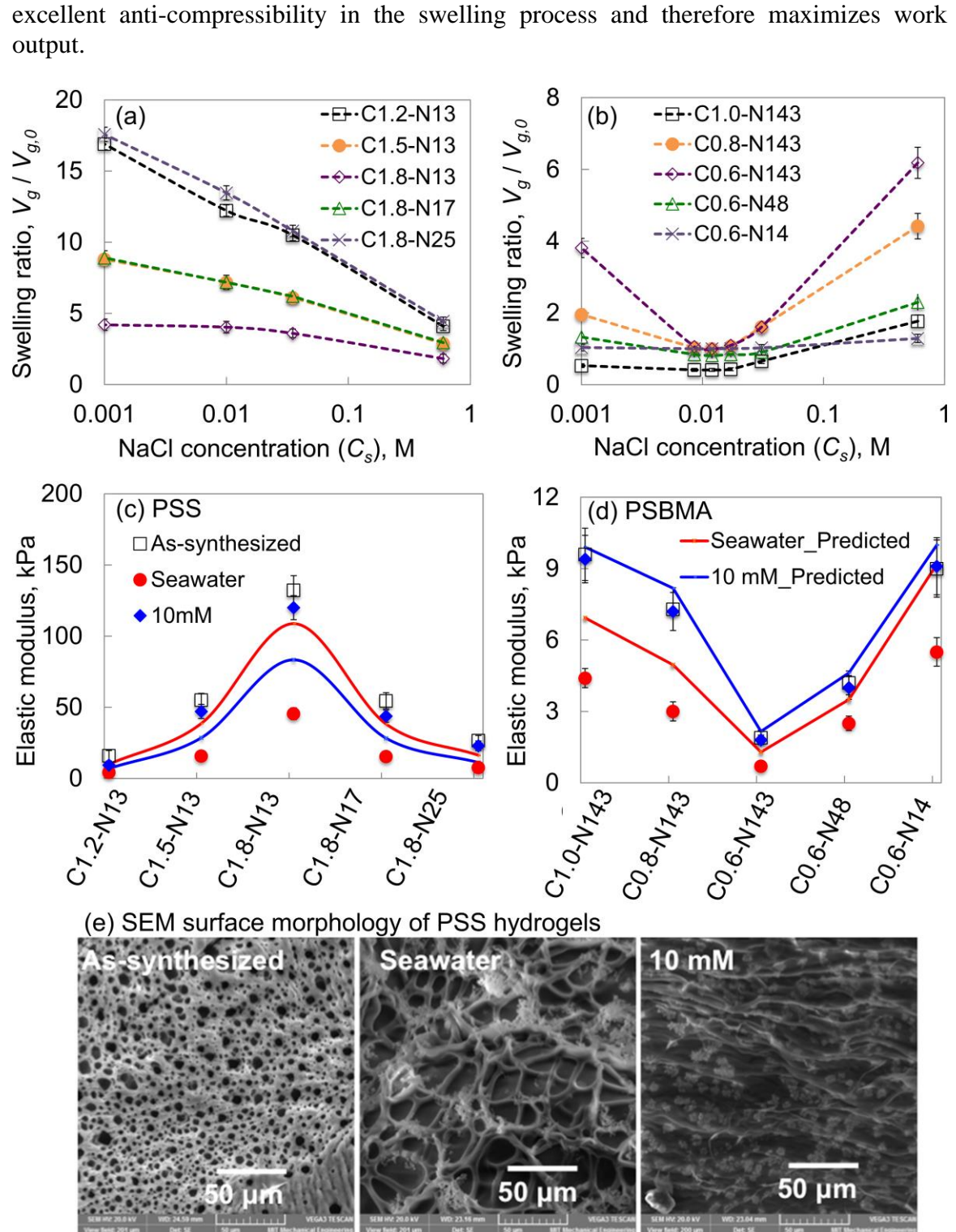

Fig. 8 The experimental equilibrium states of PSS and PSBMA hydrogels in aqueous solutions. (a) Swelling ratio of PSS gels, (b) swelling ratio of PSBMA gels, (c) elastic modulus of PSS gels, (d) elastic modulus of PSBMA gels and (e) the SEM surface

morphology of the PSS-C1.8-N25 gel in the as-synthesized, seawater and 10 mM NaCl solutions. The solid lines in (c) and (d) represent theoretical predictions of the elastic modulus of hydrogels.

Overall, the basic theoretical framework in this work qualitatively captures the experimentally measured trends and is useful in understanding the key parameters that govern the chemo-mechanical coupling in hydrogels.

4.2.2 Swelling kinetics of PSS hydrogels

Swelling kinetics determine the time scale within which the swelling / deswelling processes or an energy generation cycle is completed. It is directly related to the power output of the hydrogel system. Fig. 9a presents the diameter of hydrogel beads against time during swelling or deswelling. It shows that, for two beads whose diameters in 10 mM NaCl are 1.1 mm or 1.9 mm, the swelling or deswelling process is completed within 30 min. The smaller bead swells faster, consistent with eq. (27), which predicts that the relaxation time is inversely proportional to the square of the bead diameter. From Fig. 9b it is found that the swelling relaxation timescales of the small and large beads are around 2 min and 8 min, respectively, in good agreement with eq. (27). From these observations, the diffusivity in case of the PSS gels in NaCl solution is estimated to be around 2×10^{-9} m^2 s^{-1}.
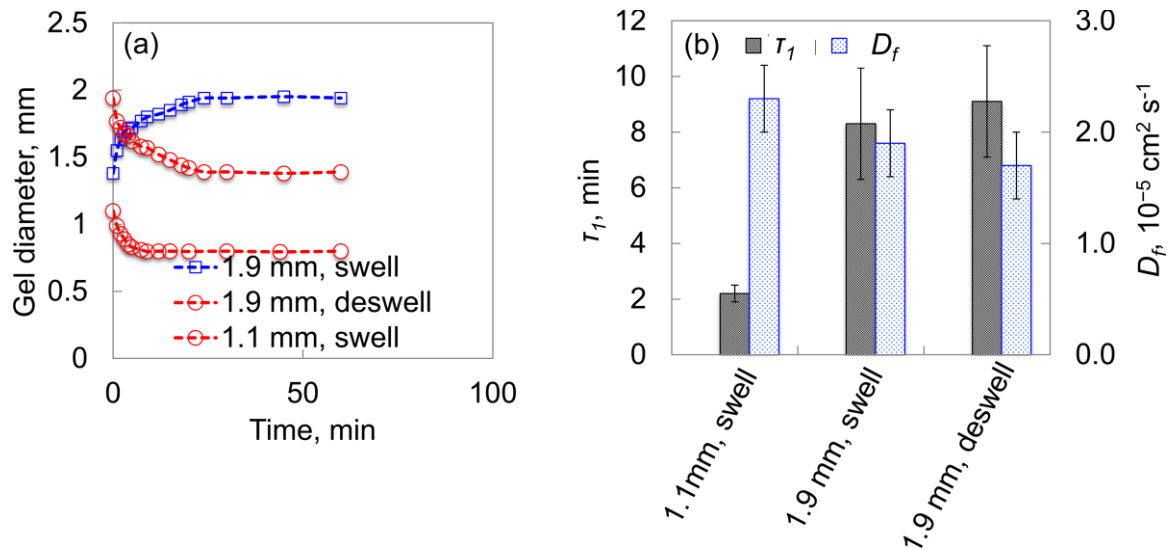
Fig. 9 (a) The change in gel diameter with time during swelling and deswelling processes (when the external bath is changed from seawater to 10 mM NaCl and vice versa) and (b) the calculated relaxation time (τ_l) and diffusivity, for 1.1 and 1.9 mm diameter PSS hydrogel beads (numbers refer to the equilibrium hydrogel diameter in seawater).

4.2.3 Demonstration of mechanical energy extraction from cyclic swelling-deswelling of PSS hydrogels

Experimental demonstration of energy conversion. The PSS-C1.8-N25 hydrogel was chosen for the demonstration of osmotic energy extraction for its good mechanical strength and reasonable swelling ratios that benefit clear lab-scale demonstrations. Although PSS-C1.8-N13 should provide a higher theoretical efficiency, a correspondingly higher pressure

that is on the same order of magnitude as the elastic modulus is necessary to achieve good efficiencies. Since the application of pressure was practically limited, the PSS-C1.8-N25 was chosen instead. The diameter of the gel beads was 400 – 800 μm in seawater (600 mM NaCl) and 550 – 1100 μm in 10 mM NaCl. The upward movement of the weights that apply mechanical force on the gel during hydrogel swelling is shown in the inserted images in Fig. 10(a). It is seen from Figs. 10(a) and 10(b) that, at a solution flow rate of 7.5 ml/min, a swelling-deswelling cycle is completed within 20 min under different applied pressures in 10 – 600 mM NaCl solutions, with good repeatability over 3 continuous cycles. The gels deswell rapidly in seawater, and then swell in 10 mM NaCl to slightly different extents for different external loads. Due to the swelling-induced gel strengthening property, the gel volume remains high even at 52.5 kPa pressure applied by the external load. Fig. 10(c) shows that the thermodynamic efficiency in terms of the work output over total released energy in one cycle and power density (per packing volume) are higher at higher applied pressures. This is in good qualitative agreement with theoretical predictions presented in Fig. 5c, which shows that the work extracted first increases with increasing pressure. Due to the strong mechanical stability of the PSS gels, the extracted work and hence efficiency are in the same magnitude but about five times higher than theoretical predictions. In addition, the applied pressure has not yet reached the latter stage where the work and efficiency start to decrease at further increased pressure as predicted in Fig. 5c and 5d, again attributing to the swelling-induced stiffening of PSS hydrogels. At 52.5 kPa, 0.95% energy efficiency and 40 W m^{-3} power density are achieved. The energy efficiency falls within the range of theoretical predictions and the power density reaches up to 10% of some PRO hollow fiber modules based on assumptions of PRO membranes with 1 W m^{-2} power density (per area)[3] and packing density of ~ 380 m^2 m^{-3} within the module. It is expected that higher efficiency and power density can be achieved by further increase in pressure and facilitating mass transport by means such as decreasing the gel bead diameter, as predicted by theoretical modeling. . For example, using beads or fibers of 300 µm diameter will reduce this timescale to ~10 s, thereby offering the possibility of considerably increasing the power density. In addition, the energy output is affected by operating parameters such as the solution flow rate and packing volume, as demonstrated in Figs. S11(a) -11(c).

High (>10%) energy efficiency at low salinity. The potential of energy production from lower salinity sources is also demonstrated as shown in Fig. 10(d) (the volume change of gels is given in Fig. S11d). The trends are also in good agreement with theoretical predictions in Fig. 6(a). Replacing 10 mM NaCl with 1 mM NaCl does not bring much change in either thermodynamic efficiency or power density. However, when brackish water sources (300 mM, 100 mM or 50 mM NaCl solutions) are employed instead of seawater, substantial improvement in energy efficiency is observed. It is noteworthy that the efficiency exceeds 10% for 50 mM NaCl, while the power density remains higher than half of that for seawater. This behavior is attributed to the more effective charge shielding effects of polyelectrolyte hydrogels at lower salt concentration and to the increasing elastic modulus of PSS hydrogels in the extensively swollen state. It suggests that polyelectrolyte hydrogels may serve as a good platform for osmotic energy production from low or moderate salinity sources. It is also noted that the energy consumption from pumping and other processes is not included in the aforementioned energy calculations; instead, this

paper focuses on the demonstration and understanding of hydrogels only. For the system and operation shown in Fig. 10, we estimate (Supplemental Material, Section 7) that the pumping loss is on the order of ~1% of the work done by the hydrogel, illustrating the feasibility of the approach. Energy conversion to electrical energy will incur additional losses, but the efficiency of mechanical to electrical energy conversion is generally quite good and exceeds 90% in many cases. Further experimental studies and system-level design and analysis are necessary in the future to fully develop the process. In addition, practical use of such energy conversion will require hydrogels that are robust under operation over a large number of cycles. Researchers have shown energy conversion using hydrogels with up to 20 cycles of operation without loss of performance[28,29], indicating potential for withstanding many cycles. However, if fatigue of hydrogels becomes a limiting factor for longer-term operation, appropriate design of hydrogels such as using porous monoliths[46] to avoid sphere-sphere contact and wear, or use of interpenetrating polymer networks to enhance toughness and fatigue resistance[42,47,48], may be required. Furthermore, fouling or loss of reversibility or ion exchange capacity of such materials will need to be assessed by conducting pilot studies using actual water samples.
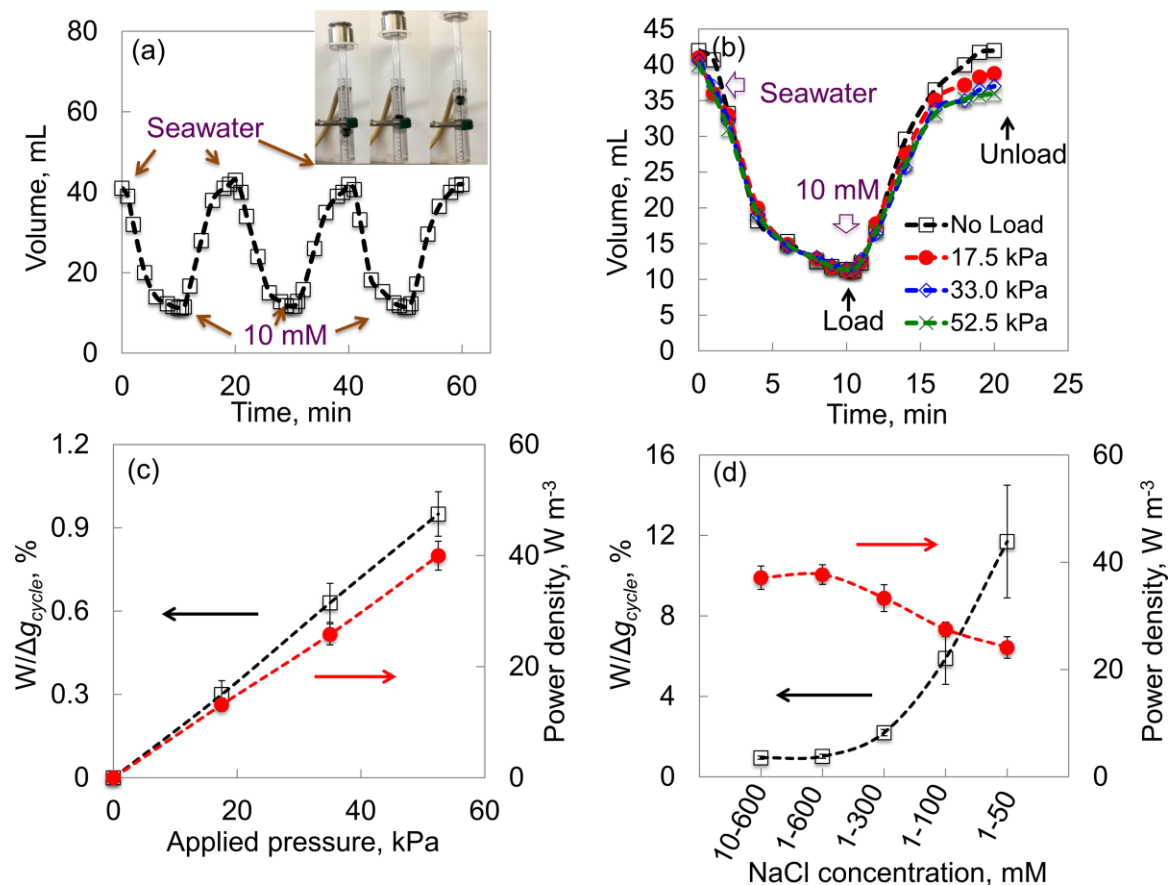
Fig. 10 (a) Change in volume of hydrogel column with time when seawater and 10 mM NaCl are alternatively flowed through the hydrogel-mechanical energy production demonstration system for 3 consecutive cycles with zero external load. Inset shows photographs of the system during the swelling process. (b) Effect of external load on the

change of hydrogel column volume with time when the seawater and 10 mM NaCl are sequentially flowed through the system. Effect of (c) applied pressure and (d) NaCl concentration on the power density (per unit packing volume) and thermodynamic efficiency. The gel volume is large (L) and flow rate of the solutions is 7.5 mL/min. Red and black curves are paired with arrows of the same color to indicate the corresponding vertical axis.

5. Conclusion

The potential of hydrogels for energy generation from salinity gradients has been investigated theoretically and experimentally, with emphasis on the chemo-mechanical coupling within hydrogels. It was demonstrated that the energy efficiency is highly dependent on the hydrogel material, which is mainly characterized by two properties, *i.e.*, charge and elastic modulus, and their interplay. Polyelectrolytes are found to be better candidates than polyampholytes for this purpose. Besides, properly designing the crosslinking density, monomer concentration, number of charge per monomer and elastic modulus may increase the thermodynamic efficiency of a zero-frictional swelling process to more than 5%. Meanwhile, the energy efficiency is also related to salinity. Due to the more sensitive response of hydrogel volume at dilute salt concentrations, higher efficiency is typically achieved at lower salinity. Further analysis of the process, e.g., the application of continuous operation, is necessary in the future work to improve the efficiency.

Experimental demonstration by PSS and PSBMA hydrogels supported the theoretical analysis. The unique swelling-strengthening mechanical property of PSS makes it an especially good candidate for energy generation. Kinetic studies revealed the fast swelling / deswelling rate of PSS gels, which suggests that power densities approaching that of PRO may be possible. Lastly, the mechanical extraction of osmotic energy was demonstrated and thermodynamic efficiency exceeding 10% was achieved.

In comparison with the PRO process for osmotic energy production, the hydrogel-based process shows relatively limited power density and is more suited for applications in the low- to medium- salinity range. However, it also offers advantages such as potentially low fouling propensity, lower operational cost and possibility for small-scale applications that enables simplicity of operation. For practical applications, the hydrogels may be packed and made into portable systems, and put in use to provide electricity when exploring remote areas. Other applications include powering of autonomous instruments in estuaries or other places where salinities change periodically.

Further development of this technology is necessary on several fronts. This work primarily investigated the most fundamental framework for material design of hydrogels, and provided a proof-of-concept device to illustrate energy harvesting. Several assumptions were made to simplify the theoretical framework, including that the partition of ions is well-described by Donnan equilibrium, that the gel is isotropic, and that the gel mechanics are described by consideration of solvation and simple entropic contribution as described by the Flory-Huggins theory. The theory may be improved in the future by taking count into the non-Gaussian chain behaviors, chain stiffening at higher strains, contributions from counter-ions, and the osmotic passivity phenomena. Modifications of the theories by taking

into account the deviations in elasticity and osmotic activity of counter-ions in different hydrogels are necessary to provide detailed, quantitative guidance for experiments.

In addition, further work is required on the design of devices and processes to fully utilize the potential of hydrogels, including downstream storage or use of the produced work. Various system and cycle designs, each with their unique advantages and disadvantages, are expected. Second, the robustness of materials needs to be characterized and optimized for repeated cycles of expansion and contraction. Finally, the utility of such systems will depend on the economics of the process. As specific material and system designs are developed, techno-economic analysis will be required to identify optimal operational conditions and to assess whether the processes are economically feasible.

Although further developments are required to advance the technology to practical applications, the results suggest the potential of harnessing chemo-mechanical coupling in engineered materials for harvesting energy from mixing processes, for chemical sensing, and to use the converse phenomena for chemical separations such as water desalination.

Acknowledgement

Supplemental Material

Detailed theoretical derivations of the chemical potential and equilibrium states of hydrogels in salt solutions; charge properties of PSBMA hydrogels; photo of the hydrogel-osmotic energy extraction device; theoretical results on free energy, swelling and solution characteristics of hydrogels in infinite and finite baths; stress-strain curves of the PSS and PSBMA hydrogels; the change of gel volume against time in the swelling-deswelling cycles of the PSS hydrogel system for osmotic energy extraction.

Data Availability Statement

The data that supports the findings of this study are available within the article and its supplementary material.

References

[1] R.E. Pattle, Nature **174**, 660 (1954).
[2] S. Loeb and R.S. Norman, Science (80-.). **189**, 654 (1975).
[3] T. Thorsen and T. Holt, J. Memb. Sci. **335**, 103 (2009).
[4] N.Y. Yip and M. Elimelech, Environ. Sci. Technol. **46**, 5230 (2012).
[5] S. Lin, A. Straub, and M. Elimelech, Energy Environ. Sci. **7**, 2706 (2014).
[6] F. Helfer, C. Lemckert, and Y.G. Anissimov, J. Memb. Sci. **453**, 337 (2014).
[7] G.L. Wick and W.R. Schmitt, Mar. Technol. Soc. J. **11**, 16 (1977).
[8] G. Micale, A. Cipollina, and A. Tamburini, in *Sustain. Energy from Salin. Gradients*, edited by A. Cipollina and G. Micale, 1st ed. (Woodhead Publishing, Cambridge, 2016), pp. 1–17.
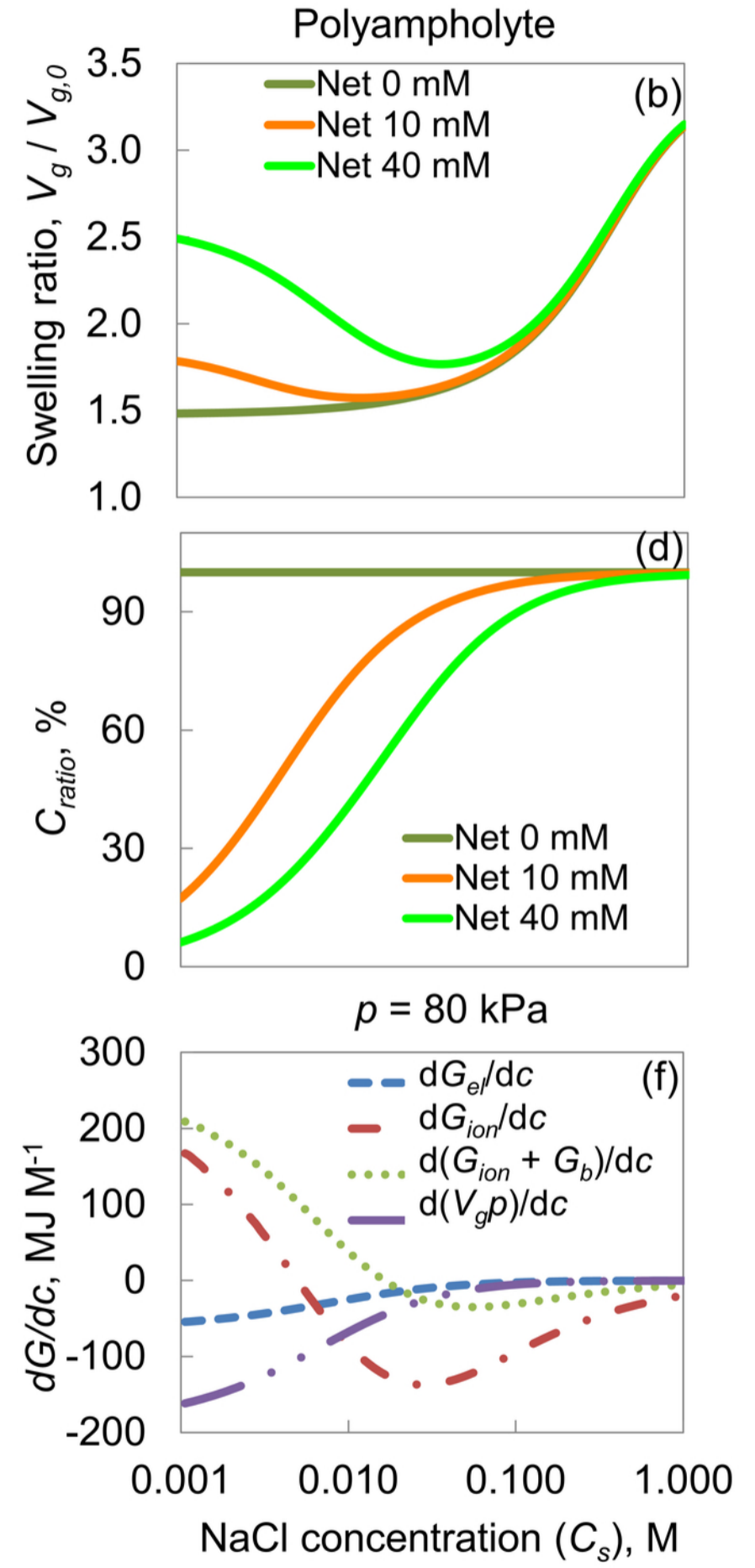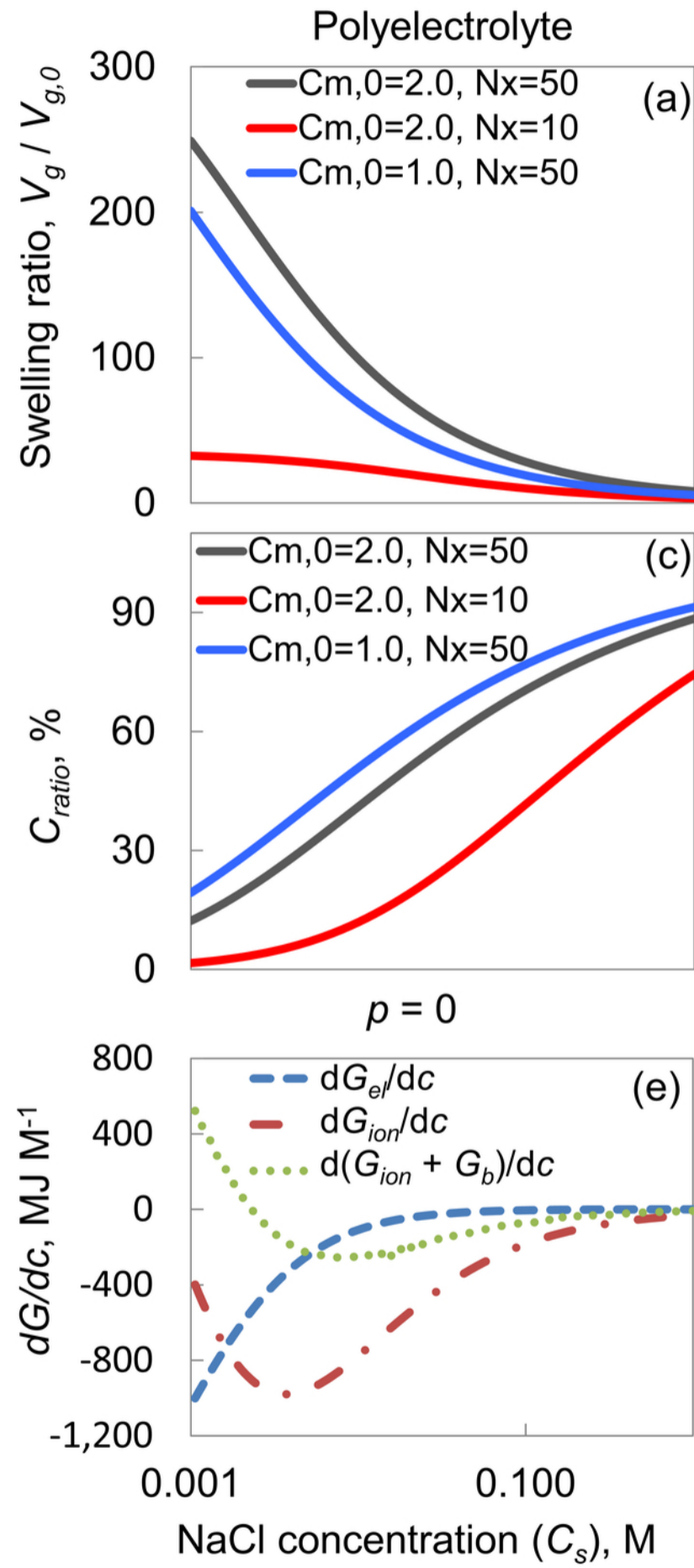[9] J. Veerman, M. Saakes, S.J. Metz, and G.J. Harmsen, Environ. Sci. Technol. **44**, 9207 (2010).

[10] J.W. Post, H.V.M. Hamelers, and C.J.N. Buisman, Environ. Sci. Technol. **42**, 5785 (2008).

[11] D. Brogioli, R. Zhao, P.M. Biesheuvel, H. Bruning, A. van der Wal, and H.V.M. Hamelers, J. Colloid Interface Sci. **332**, 258 (2009).

[12] D. Brogioli, R. Ziano, R.A. Rica, D. Salerno, O. Kozynchenko, H.V.M. Hamelers, and F. Mantegazza, Energy Environ. Sci. **5**, 9870 (2012).

[13] S. Loeb, J. Memb. Sci. **1**, 49 (1976).

[14] S. Zhang, G. Han, X. Li, C.F. Wan, and T.-S. Chung, in *Sustain. Energy from Salin. Gradients*, edited by A. Cipollina and G. Micale, 1st ed. (Woodhead Publishing, Cambridge, 2016), pp. 19–53.

[15] M. OLSSON, G.L. WICK, and J.D. ISAACS, Science (80-.). **206**, (1979).

[16] G. Han, S. Zhang, X. Li, and T.S. Chung, Prog. Polym. Sci. **51**, 1 (2014).

[17] C.F. Wan and T.S. Chung, J. Memb. Sci. **479**, 148 (2015).

[18] A.P. Straub, A. Deshmukh, and M. Elimelech, Energy Environ. Sci. **9**, 31 (2016).

[19] A. Katchalsky and I. Michaeli, J. Polym. Sci. **XV**, 69 (1955).

[20] A.E. English, S. Mafe, J.A. Manzanares, X.H. Yu, A.Y. Grosberg, and T. Tanaka, J. Chem. Phys. **104**, 8713 (1996).

[21] I. Milimouk, a. M. Hecht, D. Beysens, and E. Geissler, Polymer (Guildf). **42**, 487 (2001).

[22] A.E. English, Phase Transitions in Polyampholytic Polymers and Hydrogels, Massachusetts Institute of Technology, 1996.

[23] L. Arens, J.B. Albrecht, J. Höpfner, K. Schlag, A. Habicht, S. Seiffert, and M. Wilhelm, Macromol. Chem. Phys. **218**, 1 (2017).

[24] J. Höpfner, C. Klein, and M. Wilhelm, Macromol. Rapid Commun. **31**, 1337 (2010).

[25] F. Zhan, Z. Wang, T. Wu, Q. Dong, C. Zhao, G. Wang, and J. Qiu, J. Mater. Chem. A **6**, 4981 (2018).

[26] X. Zhu, W. Yang, M.C. Hatzell, and B.E. Logan, Environ. Sci. Technol. **48**, 7157 (2014).

[27] T.Q. Bui, V.D. Cao, N.B.D. Do, T.E. Christoffersen, W. Wang, and A.L. Kjøniksen, ACS Appl. Mater. Interfaces **10**, 22218 (2018).

[28] L. Arens, F. Weißenfeld, C.O. Klein, K. Schlag, and M. Wilhelm, Adv. Sci. **4**, (2017).

[29] S. Zavahir, I. Krupa, S.A. AlMaadeed, J. Tkac, and P. Kasak, Environ. Sci. Technol. (2019).

[30] D.W. Urry, US 5085055A (1991).

[31] P.J. Flory and J. Rehner, J. Chem. Phys. **11**, 521 (1943).

[32] P.J. Flory, *Principles of Polymer Chemistry.* (Cornell University Press, 1953).

[33] D.J. Beebe and K.S. De, J. Microelectromechanical Syst. **11**, 544 (2002).

[34] R. Skouri, F. Schosseler, J.P. Munch, and S.J. Candau, Macromolecules **28**, 197 (1995).

[35] G. Nisato, J.P. Munch, and S.J. Candau, Langmuir **15**, 4236 (1999).

[36] J.W. Tester and M. Modell, *Thermodynamics and Its Applications* (Prentice Hall PTR, 1997).

[37] S.I. Sandler, *Chemical and Engineering Thermodynamics* (Wiley, 1989).

[38] L.R.G. Treloar, *The Physics of Rubber Elasticity* (Clarendon Press, 2005).

[39] A. Katchalsky, J. Polym. Sci. **XV**, 69 (1955).

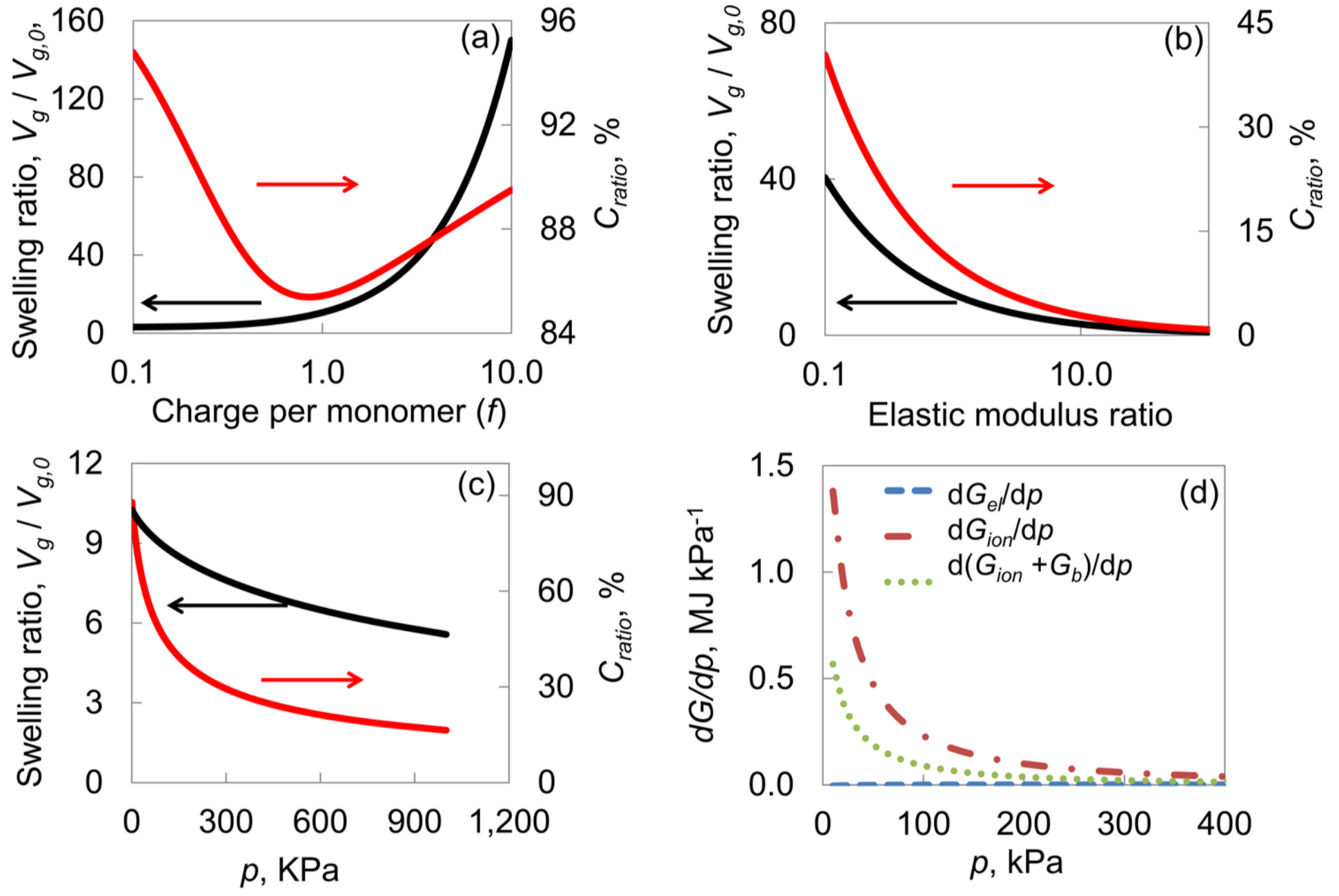[40] Y. Li and T. Tanaka, J. Chem. Phys. **92**, 1365 (1990).

[41] T. Tanaka and D.J. Fillmore, J.Chem. Phys. **70**, 1214 (1979).

[42] J.-Y. Sun, X. Zhao, W.R.K. Illeperuma, O. Chaudhuri, K.H. Oh, D.J. Mooney, J.J. Vlassak, and Z. Suo, Nature **489**, 133 (2012).

[43] M.A. Haque, T. Kurokawa, and J.P. Gong, Polymer (Guildf). **53**, 1805 (2012).

[44] F. Horkay, F. Horkay, I. Tasaki, I. Tasaki, P.J. Basser, and P.J. Basser, Biomacromolecules **1**, 84 (2000).

[45] K.B. Zeldovich and A.R. Khokhlov, Macromolecules **32**, 3488 (1999).

[46] F. Svec, J. Chromatogr. A **1217**, 902 (2010).

[47] S. Lin, X. Liu, J. Liu, H. Yuk, H.-C. Loh, G.A. Parada, C. Settens, J. Song, A. Masic, G.H. Mckinley, and X. Zhao, *Anti-Fatigue-Fracture Hydrogels* (2019).

[48] C. Xu, G. Dai, and Y. Hong, Acta Biomater. **95**, 50 (2019).

36

(a)

Gel β

Bath α
(C_α)

Bath β
(C_β)

Immersion into bath α

Bath α (f)
$(C_{\alpha,f})$

Gel α

Bath β
(C_β)

**Swell,
Mixing of salts and water**

Starting state

**Free energy release
during mixing (Δg,
final – starting)**

**Process I:
Mixing** (no external
pressure, no work)

Immersion into bath β

Gel β

Bath α (f)
$(C_{\alpha,f})$

Bath β (f)
$(C_{\beta,f})$

Bath α (f)
$(C_{\alpha,f})$

Bath β (f)
$(C_{\beta,f})$

Gel β

Final state

**Deswell,
Mixing of salts and water**

(b)

Bath α
(C_α)

p

**Process II:
Maximum work
@ zero friction**
(applied pressure
varies from high to
zero, maintaining
mechanical
equilibrium)

*Immersion into bath α
Applying changing p*

(c) **Process III:
Mechanical work at constant pressure**
(fixed pressure applied during swelling,
and then released)

Bath α
(C_α)

Bath β (p)
$(C_{\beta,p})$

Gel (p)

Equilibrium

Applying constant p   *Immersion into bath α
under pressure*

Bath α (p)
$(C_{\alpha,p})$

Gel α (p)

p

Bath β (p)
$(C_{\beta,p})$

Swell

Release of pressure

(d)   Linear electricity generator

**Weight
(constant pressure)**

Hydrogel

Bath α

Bath β

Bulb

Polyelectrolyte

Polyampholyte

(a) Δg_{cycle}, MJ m^{-3}

(b) Δg_{cycle}, MJ m^{-3}

(c) W_{max}, MJ m^{-3}

(d) W_{max}, MJ m^{-3}

(e) $\eta_{m/swell}$, %

(f) $\eta_{m/swell}$, %

(g) $\eta_{m/cycle}$, %

(h) $\eta_{m/cycle}$, %

N_x

$C_{m,0}$, M

(a) Work at constant p

Work, W, MJ m^{-3}

(b) Work ratio (W / W_{max})

WR (W / W_{max}), %

Cm,0=2.0, Nx=10
Cm,0=2.0, Nx=50
Cm,0=3.0, Nx=10

p, kPa

(a) $C_{s,\alpha}$ = 10 mM

(b) $C_{s,\beta}$ = 600mM

(a)

C1.2-N13
C1.5-N13
C1.8-N13
C1.8-N17
C1.8-N25

(b)

C1.0-N143
C0.8-N143
C0.6-N143
C0.6-N48
C0.6-N14

Swelling ratio, $V_g / V_{g,0}$

NaCl concentration (C_s), M

(c) PSS

As-synthesized
Seawater
10mM

(d) PSBMA

Seawater_Predicted
10 mM_Predicted

Elastic modulus, kPa

(e) SEM surface morphology of PSS hydrogels

As-synthesized   Seawater   10 mM

50 μm   50 μm   50 μm